

# Self-Normalized Quantile Empirical Saddlepoint Approximation

HOU Jian<sup>1</sup>, MENG Tan<sup>1</sup>, and TIAN Maozai\*<sup>1</sup>

<sup>1</sup>Center for Applied Statistics, School of Statistics,  
Renmin University of China, Beijing 100872, China

## Abstract

We propose a density-free method for frequentist inference on population quantiles, termed *Self-Normalized Quantile Empirical Saddlepoint Approximation* (SNQESA). The approach builds a self-normalized pivot from the indicator score for a fixed quantile threshold and then employs a constrained empirical saddlepoint approximation to obtain highly accurate tail probabilities. Inverting these tail areas yields confidence intervals and tests without estimating the unknown density at the target quantile, thereby eliminating bandwidth selection and the boundary issues that affect kernel-based Wald/Hall-Sheather intervals. Under mild local regularity, the resulting procedures attain higher-order tail accuracy and second-order coverage after inversion. Because the pivot is anchored in a bounded Bernoulli reduction, the method remains reliable for skewed and heavy-tailed distributions and for extreme quantiles. Extensive Monte Carlo experiments across light, heavy and multimodal distributions demonstrate that SNQESA delivers stable coverage and competitive interval lengths in small to moderate samples while being orders of magnitude faster than large- $B$  resampling schemes. An empirical study on Value-at-Risk with rolling windows further highlights the gains in tail performance and computational efficiency. The framework naturally extends to two-sample quantile differences and to regression-type settings, offering a practical, analytically transparent alternative to kernel, bootstrap, and empirical-likelihood methods for distribution-free quantile inference.

**Keywords:** Quantile Inference, Saddlepoint Approximation, Self-Normalization, Density-free, Confidence Intervals

## 1 Introduction

Quantiles provide fundamental characterizations of distributional features, with wide application across economics, finance, biostatistics, and engineering for measuring location, tail risk, and inequality. Despite their prevalence, frequentist inference for population quantiles presents persistent challenges: the asymptotic variance of sample quantiles depends on the unknown density at the target quantile, which proves difficult to estimate accurately in small samples, with skewed or heavy-tailed distributions, or near distributional extremes. Classical kernel-based Wald and Hall-Sheather (HS) intervals, while widely used, exhibit sensitivity to bandwidth selection and boundary effects, often producing erratic coverage and unstable interval lengths in finite samples (Hall and Sheather, 1988; Sheather and Jones, 1991; Sheather, 2004; Hyndman and Fan, 1996).

Bootstrap methods offer appealing alternatives through their general applicability and conceptual simplicity, including percentile and BCa intervals (Efron, 1987; Efron and Tibshirani, 1993; Davison and Hinkley, 1997). However, bootstrap procedures can be computationally demanding and may perform inadequately for extreme quantiles or irregular problems. Refinements like subsampling and  $m$ -out-of- $n$  bootstrap have been proposed to enhance robustness in these settings (Politis et al., 1999; Bickel and Sakov, 2008). Empirical likelihood (EL) constitutes another influential approach, preserving attractive likelihood-based properties without parametric specification. For quantile inference, smoothed EL achieves higher-order accuracy under regularity conditions, though implementations may encounter numerical difficulties from convex hull constraints and require additional smoothing decisions (Chen and Hall, 1993; Owen, 2001).

Saddlepoint methods provide an alternative pathway, delivering exceptional accuracy in small-sample tail approximations through exploitation of cumulant generating functions (CGFs). The celebrated

---

\*CONTACT. Author Email: [mztian@ruc.edu.cn](mailto:mztian@ruc.edu.cn)

Lugannani-Rice (LR) approximation and Barndorff-Nielsen  $r^*$  correction exemplify this approach (Daniels, 1954; Lugannani and Rice, 1980; Barndorff-Nielsen, 1986; Brazzale et al., 2007). When population CGFs are unavailable, empirical saddlepoint approximation (ESA) substitutes the empirical CGF, extending saddlepoint accuracy to nonparametric contexts (Feuerverger, 1989), with recent work clarifying estimation and implementation aspects (Holcblat and Vitale, 2022). Concurrently, self-normalization (SN) has emerged as a powerful framework for constructing pivots that circumvent explicit scale estimation while maintaining stability under heterogeneity and heavy tails, with extensive development for both independent and dependent data (de la Peña et al., 2009; Shao, 2010, 2015).

Recent methodological developments further underscore the relevance of saddlepoint-based, density-free approaches. Saddlepoint techniques continue to provide accurate small-sample  $p$ -values beyond classical parametric settings, including spatial panel data models, discrete GLM score tests with rare events, and nonparametric rank-type procedures, reflecting both analytical tractability and numerical stability in modern implementations (Jiang et al., 2023; Ko et al., 2022; Abd El-Raheem et al., 2023). The self-normalization paradigm has seen renewed development for change-point detection and robust testing, reinforcing the value of pivots that avoid explicit scale estimation under heterogeneity or heavy tails (Cheng and Chan, 2024). For extreme quantiles in regression, recent advances address high-dimensional and persistent-regressor environments, complementing our distribution-free perspective for i.i.d. settings (Liu et al., 2024). These developments provide broader context for the current SNQESA proposal and its extensions to regression-type designs, where constrained ESA with rank-reduced curvature remains effective.

This paper introduces SNQESA for density-free quantile inference. We observe that the score function for a fixed quantile threshold takes only two values; self-normalizing the score sum by its internal quadratic form yields a pivotal statistic whose null distribution remains independent of the unknown quantile density. Leveraging this structure, we employ constrained saddlepoint arguments to approximate the self-normalized statistic's tail probability with LR/ $r^*$ -type accuracy, then invert the resulting  $p$ -values to construct confidence intervals. Unlike kernel-based Wald/HS intervals, our approach completely eliminates bandwidth selection. Compared to bootstrap and EL methods, it provides an analytical, non-resampling solution with higher-order small-sample accuracy and competitive or superior performance for tail quantiles.

#### Contributions.

1. **Density-free accurate quantile inference.** We develop a self-normalized pivot specifically for quantile testing and derive ESA-based LR/ $r^*$  tail approximations that produce precise  $p$ -values without estimating  $f(q_\tau)$ . The method maintains computational efficiency and stability in small samples and at extreme quantiles.
2. **Higher-order guarantees.** Under mild regularity conditions, the proposed tail approximations achieve the higher-order accuracy characteristic of saddlepoint methods, while interval inversion delivers second-order coverage improvements typical of LR/ $r^*$  calibrations (Barndorff-Nielsen, 1986; Brazzale et al., 2007).
3. **Robustness to distributional characteristics.** Self-normalization reduces sensitivity to unknown scale and tail behavior, aligning with recent advances advocating SN procedures in non-Gaussian, dependent, or heteroskedastic environments (Shao, 2010, 2015).
4. **Extensibility.** The framework naturally extends to two-sample quantile differences and regression-type settings, complementing developments for extremal quantiles that employ extreme-value approximations (Chernozhukov et al., 2011, 2017; Koenker, 2005).

Empirical evaluations across diverse distributions—including skewed, heavy-tailed, and multimodal cases—and spanning moderate to extreme quantiles demonstrate that our method provides stable coverage and competitive interval lengths relative to kernel-based Wald/HS, smoothed EL, and bootstrap variants, while achieving substantial computational speed advantages over resampling methods. These results, combined with the method's transparency and straightforward implementation, position SNQESA as a practical default for distribution-free quantile inference in small to moderate samples.

## 2 Method

This section develops a density-free procedure for quantile inference that combines a self-normalized pivot with a constrained empirical saddlepoint approximation (ESA). Let  $X_1, \dots, X_n$  be an i.i.d. draws

from a continuous distribution  $F$ , fix  $\tau \in (0, 1)$ , and denote the target quantile by  $q_\tau = F^{-1}(\tau)$ . For any threshold  $t \in \mathbb{R}$  define  $Y_i(t) = \mathbf{1}\{X_i \leq t\}$  and the two-point score

$$\psi_\tau(X_i; t) = \tau - Y_i(t) \in \{\tau - 1, \tau\}.$$

Write the partial sum, the sum of squares and the self-normalized statistic as

$$S_n(t) = \sum_{i=1}^n \psi_\tau(X_i; t), \quad Q_n(t) = \sum_{i=1}^n \psi_\tau^2(X_i; t), \quad T_n(t) = \frac{S_n(t)}{\sqrt{Q_n(t)}}. \quad (1)$$

Under the simple null  $H_0 : F(t) = \tau$ ,  $Y_i(t) \stackrel{\text{i.i.d.}}{\sim} \text{Bernoulli}(\tau)$ , hence the joint distribution of  $(S_n(t), Q_n(t))$  is free of the unknown density  $f(q_\tau)$ . Let  $W_i(t) = (\psi_\tau(X_i; t), \psi_\tau^2(X_i; t))^\top$ . Then  $W_i$  takes two support points

$$\begin{aligned} w_1 &= (\tau - 1, (1 - \tau)^2)^\top \text{ with prob. } \tau, \\ w_0 &= (\tau, \tau^2)^\top \text{ with prob. } 1 - \tau, \end{aligned}$$

and its one-observation moment generating function (MGF) and cumulant generating function (CGF) are

$$M(\lambda) = \tau e^{\lambda_1(\tau-1) + \lambda_2(1-\tau)^2} + (1 - \tau) e^{\lambda_1\tau + \lambda_2\tau^2}, \quad K(\lambda) = \log M(\lambda), \quad \lambda = (\lambda_1, \lambda_2)^\top.$$

Introduce the tilted success probability

$$p_\lambda = \frac{\tau e^{\lambda_1(\tau-1) + \lambda_2(1-\tau)^2}}{\tau e^{\lambda_1(\tau-1) + \lambda_2(1-\tau)^2} + (1 - \tau) e^{\lambda_1\tau + \lambda_2\tau^2}} \in (0, 1), \quad (2)$$

so that the unit-scale gradient and Hessian take the rank-1 form

$$\begin{aligned} \mu(\lambda) &= \nabla K(\lambda) = (\tau - p_\lambda, \tau^2 + p_\lambda(1 - 2\tau))^\top, \\ \Sigma(\lambda) &= \nabla^2 K(\lambda) = p_\lambda(1 - p_\lambda)vv^\top, \\ v &= w_1 - w_0 = (-1, 1 - 2\tau)^\top. \end{aligned} \quad (3)$$

Thus  $\text{rank}\Sigma(\lambda) = 1$  with image  $\text{span}(v)$ ; all curvature computations reduce to this one-dimensional subspace via pseudo-determinants and the Moore-Penrose inverse. We adopt a two-dimensional constrained ESA in  $W_i(t)$  because the rank-1 geometry yields closed-form curvature and LR quantities and provides a unified, robust engine for weighted, regression, and dependent designs where a one-parameter reduction is unavailable. In the i.i.d. case considered here, it reduces algebraically to the one-parameter binomial tilt recorded below.

Let the observed value be the signed statistic

$$x_{\text{obs}}(t) = \frac{S_n(t)}{\sqrt{Q_n(t)}},$$

and impose the boundary in the observed direction through

$$g(s, q) = s - x_{\text{obs}}\sqrt{q}.$$

Following the constrained formulation of [Skovgaard \(2001\)](#) (see also [Brazzale et al., 2007](#)), the most likely point where the tilted mean hits the boundary solves

$$n\nabla K(\hat{\lambda}) = \hat{\mu} = (\hat{s}, \hat{q})^\top, \quad g(\hat{s}, \hat{q}) = 0, \quad \hat{\lambda} = \hat{\eta}\nabla g(\hat{\mu}), \quad (4)$$

with  $J(\lambda) = n\nabla^2 K(\lambda) = np_\lambda(1 - p_\lambda)vv^\top$  and

$$\nabla g(\mu) = \left(1, -\frac{x_{\text{obs}}}{2\sqrt{\mu_2}}\right)^\top.$$

Using the unit-scale CGF  $K$ , we define the deviance and signed root on the sum scale

$$D_{\text{sum}} = 2n\{\hat{\lambda}^\top \mu(\hat{\lambda}) - K(\hat{\lambda})\}, \quad r = \text{sgn}(\hat{\eta})\sqrt{D_{\text{sum}}}. \quad (5)$$

Equivalently, if  $D = 2\{\hat{\lambda}^\top \mu(\hat{\lambda}) - K(\hat{\lambda})\}$  is the unit-scale deviance, then  $D_{\text{sum}} = nD$  and  $r = \text{sgn}(\hat{\eta})\sqrt{nD}$ ; we work with  $D_{\text{sum}}$  to align with common saddlepoint conventions. Since under  $H_0$  the pivot is a discrete transform of a binomial count, we evaluate directed tails by default with a mid- $p$  modification

$$p_{\text{mid}}(t) = \mathbb{P}\{T_n(t) > x_{\text{obs}}(t)\} + \frac{1}{2}\mathbb{P}\{T_n(t) = x_{\text{obs}}(t)\},$$

or with a small Cornish-Fisher continuity shift; both preserve the third-order tail accuracy and the  $O(n^{-1})$  coverage after inversion (see [Daniels, 1954](#); [Lugannani and Rice, 1980](#); [Barndorff-Nielsen, 1986](#); [Brazzale et al., 2007](#)).

The directed one-sided tail, namely the upper tail if  $x_{\text{obs}} \geq 0$  and the lower tail if  $x_{\text{obs}} < 0$ , is approximated by the Barndorff-Nielsen correction

$$r^* = r + \frac{1}{r} \log \frac{r}{w}, \quad p_{\text{dir}}(t) \approx \Phi(-\text{sgn}(x_{\text{obs}})r^*), \quad (6)$$

where the curvature factor reduces from Skovgaard's general rank-1 form to a closed expression. Since  $J = n\Sigma$  with  $\text{pdet}(J) = np_{\hat{\lambda}}(1-p_{\hat{\lambda}})\|v\|^2$  and  $\Sigma(\hat{\lambda})^+ = \{p_{\hat{\lambda}}(1-p_{\hat{\lambda}})\}^{-1}vv^\top/\|v\|^4$ , we obtain

$$w = |\hat{\eta}|\sqrt{np_{\hat{\lambda}}(1-p_{\hat{\lambda}})} \frac{\|v\|^3 \|\nabla g(\hat{\mu})\|}{|\nabla g(\hat{\mu}) \cdot v|}. \quad (7)$$

We also define the signed Lugannani-Rice quantity

$$q^\pm = (\text{logit}(\hat{p}) - \text{logit}(\tau))\sqrt{n\hat{p}(1-\hat{p})}. \quad (8)$$

When  $|\log(r/w)| \leq c_0$  (default  $c_0 = 2$ ) we use the  $r^*$  tail; otherwise we fall back to the signed Lugannani-Rice expansion

$$p_{\text{dir}}(t) \approx \Phi(-\text{sgn}(x_{\text{obs}})r) + \phi(r) \left( \frac{1}{r} - \frac{1}{q^\pm} \right). \quad (9)$$

A two-sided  $p$ -value is finally reported as

$$p_{\text{two-sided}}(t) = 2 \min\{p_{\uparrow}(t), p_{\downarrow}(t)\}, \quad p_{\uparrow}(t) = \mathbb{P}\{T_n(t) \geq x_{\text{obs}}\}, \quad p_{\downarrow}(t) = \mathbb{P}\{T_n(t) \leq x_{\text{obs}}\}. \quad (10)$$

For numerical stability we enforce a degeneracy check  $|\nabla g(\hat{\mu}) \cdot v| > \delta$  (we use  $\delta = 10^{-10}$ ); if violated we revert to the one-parameter evaluation at  $u_x$  defined below and compute  $r, q^\pm, r^*$  from the binomial tilt (in that branch  $w = q^\pm$ ). In the constrained solver we bound  $|\hat{\eta}|$  via trust-region damping and a backtracking line search to avoid overflow when  $\nabla g(\hat{\mu}) \cdot v$  is near zero.

We now record an algebraic reduction to a one-parameter binomial tilt and the induced equality of tilts. With  $\bar{Y}_n(t) = n^{-1} \sum_{i=1}^n Y_i(t)$  there exists a strictly monotone map

$$T_n(t) = h(\bar{Y}_n(t)), \quad h(u) = \frac{\sqrt{n}(\tau - u)}{\sqrt{u(1-\tau)^2 + (1-u)\tau^2}},$$

so that  $\{T_n(t) \geq x_{\text{obs}}\}$  is equivalent to  $\{\bar{Y}_n(t) \leq u_x\}$  with  $u_x = h^{-1}(x_{\text{obs}})$ . At the constrained solution we have  $\hat{\mu} = (\tau - \hat{p}, \tau^2 + \hat{p}(1-2\tau))^\top$  and the boundary  $g(\hat{\mu}) = 0$  reads

$$\tau - \hat{p} = x_{\text{obs}}\sqrt{\tau^2 + \hat{p}(1-2\tau)}.$$

Hence  $h(\hat{p}) = x_{\text{obs}}$  and, by strict monotonicity of  $h$ , we obtain the identity of tilts

$$\hat{p} = p_{\hat{\lambda}} = u_x.$$

Consequently, the scalars  $(r, q^\pm, r^*)$  computed from the constrained ESA coincide with their one-parameter binomial counterparts at  $u_x$ , which explains the third-order tail accuracy and provides a numerically robust one-dimensional fallback. Standard one-parameter saddlepoint theory for exponential families (including lattice cases with continuity corrections) yields  $O(n^{-3/2})$  relative error for directed tails, and inversion then implies  $O(n^{-1})$  endpoint perturbations and coverage error (see [Daniels, 1954](#); [Lugannani and Rice, 1980](#); [Barndorff-Nielsen, 1986](#); [Brazzale et al., 2007](#)); in our setting this transfers through the Bernoulli two-point representation and self-normalization without additional assumptions (cf. [de la Peña et al., 2009](#); [Shao, 2010, 2015](#)).

Inversion delivers confidence limits. Let  $p_{\uparrow}(t)$  and  $p_{\downarrow}(t)$  denote the directed upper and lower tails defined above. The equal-tailed  $(1 - \alpha)$  interval is obtained by solving

$$p_{\downarrow}(t_L) = \alpha/2, \quad p_{\uparrow}(t_U) = \alpha/2,$$

using monotonicity of  $p_{\downarrow}$  on  $(-\infty, \hat{q}_{\tau}]$  and of  $p_{\uparrow}$  on  $[\hat{q}_{\tau}, \infty)$ . Bracketing on a coarse grid that expands outward from the sample quantile  $\hat{q}_{\tau}$  followed by bisection to a tight tolerance is effective in practice. With ties or discretization we use the mid- $p$  modification or a Cornish-Fisher continuity shift; both preserve the  $O(n^{-1})$  coverage error when combined with the third-order tail accuracy of the ESA.

A few numerical safeguards complete the method. To avoid boundary singularities for extreme quantiles or very small  $n$ , we add a vanishing ridge to  $Q_n$ ,

$$Q_n(t) \leftarrow Q_n(t) + \epsilon_n, \quad \epsilon_n \rightarrow 0, \quad (11)$$

and in practice set  $\epsilon_n = cn^{-1/2}$  with a small constant  $c$ , which yields  $x_{\text{obs}}^{(\text{ridge})} - x_{\text{obs}} = O_p(n^{-3/2})$  and does not affect either the third-order tail accuracy or the  $O(n^{-1})$  coverage. The constrained system is solved by a damped Newton or trust-region iteration; because  $J(\lambda)$  is rank-1, each linear step reduces to one-dimensional algebra along  $v$  and is solved stably using pseudo-determinants  $\text{pdet}(\Sigma(\lambda)) = p_{\lambda}(1 - p_{\lambda})\|v\|^2$  and the Moore-Penrose inverse  $\Sigma(\lambda)^+ = \{p_{\lambda}(1 - p_{\lambda})\}^{-1}vv^T/\|v\|^4$ . The closed form of  $w$  above follows from the rank-1 projection and the identities for  $\text{pdet}(J)$  and  $\Sigma^+$ ; when the degeneracy check fails we use the one-parameter binomial evaluation at  $u_x$  for both  $r^*$  and LR tails.

### 3 Theoretical properties

We establish the accuracy of the tail approximation produced by the self-normalized empirical saddlepoint method in Section 2, and quantify the coverage error of the confidence intervals obtained by inversion. Throughout we work under the following regularity conditions.

(A1) Identification at the target quantile.  $F$  is strictly increasing at  $q_{\tau} = F^{-1}(\tau)$ ; there exists a neighborhood  $\mathcal{N}(q_{\tau})$  with  $0 < \inf_{t \in \mathcal{N}(q_{\tau})} f(t) \leq \sup_{t \in \mathcal{N}(q_{\tau})} f(t) < \infty$ .

(A2) CGF regularity and interior solvability. For the two-point score  $\psi_{\tau}(X_i; t) = \tau - \mathbf{1}\{X_i \leq t\}$  and its quadratic companion, the bivariate cumulant generating function  $K(\lambda)$  exists on  $\mathbb{R}^2$ , is  $C^3$ , strictly convex and steep; for each  $t \in \mathcal{N}(q_{\tau})$  the saddlepoint equations  $\nabla K(\lambda) = m(t)$  admit a unique solution with  $\lambda(t)$  in the interior of the natural parameter space.

(A3) Sampling and weak dependence. Either i.i.d. sampling, or strictly stationary  $\alpha$ -mixing with standard summability and finite  $(2+\delta)$ th moments for the quadratic score; the processes  $\{\psi_{\tau}(X_i; t), \psi_{\tau}^2(X_i; t)\}$  are uniformly integrable on  $\mathcal{N}(q_{\tau})$ .

(A4) Local uniformity. Uniform LLN and stochastic equicontinuity hold for  $t \mapsto n^{-1} \sum_{i=1}^n g_t(X_i)$  with  $g_t \in \{\psi_{\tau}(\cdot; t), \psi_{\tau}^2(\cdot; t)\}$  on a shrinking neighborhood  $\mathcal{N}_n(q_{\tau}) \downarrow \{q_{\tau}\}$ ; the solution  $t \mapsto \lambda_n(t)$  varies continuously on  $\mathcal{N}_n(q_{\tau})$ .

(A5) Numerical well-posedness. The empirical saddlepoint and endpoint inversion problems are well-posed and have unique solutions; the numerical solver attains them within tolerance  $o(n^{-1})$  and stays in the feasible parameter region.

(A1) is the standard identification condition for quantile inference and underlies local expansions around  $q_{\tau}$  (Koenker and Bassett, 1978; Koenker, 2005; Serfling, 1980). (A2) collects the classical regularity requirements that guarantee existence/uniqueness of the saddlepoint and justify Lugannani–Rice/ $r^*$  accuracy for tail probabilities (Daniels, 1954; Lugannani and Rice, 1980; Jensen, 1995; Butler, 2007; Reid, 2003; Kolassa, 2006). (A3) allows either i.i.d. data or short-range dependence; with a bounded score, only mild moment and mixing conditions are needed, and self-normalized limit theory applies (Jing et al., 2003; de la Peña et al., 2009; Shao, 2010; Doukhan, 1994; Rio, 2000). (A4) provides the uniform empirical-process control required to move from pointwise to uniform statements in a neighborhood of  $q_{\tau}$  (van der Vaart and Wellner, 1996; Jensen, 1995). (A5) ensures that numerical error is asymptotically negligible relative to the  $O(n^{-1})$  analytical remainder in saddlepoint approximations (Butler, 2007; Kolassa, 2006; Reid, 2003).

For a fixed threshold  $t \in \mathbb{R}$  we keep the notation from Section 2:

$$Y_i(t) = \mathbf{1}\{X_i \leq t\}, \quad S_n(t) = \sum_{i=1}^n (\tau - Y_i(t)), \quad Q_n(t) = \sum_{i=1}^n (\tau - Y_i(t))^2, \quad T_n(t) = \frac{S_n(t)}{\sqrt{Q_n(t)}},$$

and the observed value is  $x_{\text{obs}}(t) = T_n(t)$ . Under the simple null  $H_0 : F(t) = \tau$ ,  $Y_i(t)$  are i.i.d. Bernoulli( $\tau$ ). We also use the unit-scale CGF  $K(\lambda)$  and its rank-1 derivatives summarized in Section 2. The directed one-sided tail is

$$p_{\text{dir}}(t) = \begin{cases} \mathbb{P}\{T_n(t) \geq x_{\text{obs}}(t)\}, & x_{\text{obs}}(t) \geq 0, \\ \mathbb{P}\{T_n(t) \leq x_{\text{obs}}(t)\}, & x_{\text{obs}}(t) < 0, \end{cases}$$

and the two-sided value is  $p_{\text{two-sided}}(t) = 2 \min\{p_{\uparrow}(t), p_{\downarrow}(t)\}$ .

A basic reduction connects  $T_n(t)$  with the binomial sample mean  $\bar{Y}_n(t) = n^{-1} \sum_{i=1}^n Y_i(t)$  via a strictly monotone transform. Define

$$h(u) = \frac{\sqrt{n}(\tau - u)}{\sqrt{u(1-\tau)^2 + (1-u)\tau^2}}, \quad d(u) = \tau^2 + u(1-2\tau). \quad (12)$$

Elementary algebra shows  $h'(u) = -\sqrt{n}\{(1-2\tau)u + \tau\}/\{2d(u)^{3/2}\} < 0$  for  $u \in (0, 1)$  and hence the following holds.

**Lemma 1** (Binomial reduction). *Under  $H_0 : F(t) = \tau$ , one has  $T_n(t) = h(\bar{Y}_n(t))$ . In particular, for any real  $x$ , writing  $u_x = h^{-1}(x) \in (0, 1)$ , the event  $\{T_n(t) \geq x\}$  is equivalent to  $\{\bar{Y}_n(t) \leq u_x\}$ .*

The reduction allows us to adopt the one-parameter binomial saddlepoint scalars in a signed form. Let

$$r = \text{sgn}(u_x - \tau) \sqrt{2n\text{KL}(u_x \|\tau)}, \quad q^{\pm} = (\text{logit}(u_x) - \text{logit}(\tau)) \sqrt{n u_x (1 - u_x)}, \quad (13)$$

where  $\text{KL}(u \|\tau) = u \log\{u/\tau\} + (1-u) \log\{(1-u)/(1-\tau)\}$ . In our constrained rank-1 construction the solution satisfies  $\hat{p} = p_{\hat{\lambda}} = u_x$ , and the signed root deviance and the Barndorff-Nielsen correction coincide with their binomial counterparts. Writing

$$D = 2\{\hat{\lambda}^{\top} \mu(\hat{\lambda}) - K(\hat{\lambda})\}, \quad r = \text{sgn}(\hat{\eta}) \sqrt{nD}, \quad r^* = r + \frac{1}{r} \log \frac{r}{w}, \quad (14)$$

and recalling that  $\hat{p} = u_x$ , we obtain third-order tail accuracy.

**Theorem 1** (Third-order accuracy of the directed tail). *Assume (A1)-(A4). Fix a bounded  $x$  and suppose the constrained solution exists with  $\hat{p} \in (0, 1)$  bounded away from the endpoints. Under  $H_0 : F(t) = \tau$ , uniformly on compact  $x$ -sets,*

$$p_{\text{dir}}(t) = \Phi(-\text{sgn}(x)r^*)\{1 + O(n^{-3/2})\}. \quad (15)$$

Equivalently, with the signed Lugannani-Rice quantity  $q^{\pm}$  in (13), the directed tail satisfies the signed LR form

$$p_{\text{dir}}(t) = \begin{cases} \Phi(r) + \phi(r) \left( \frac{1}{r} - \frac{1}{q^{\pm}} \right) + O(n^{-3/2}), & x \geq 0, \\ \Phi(-r) + \phi(r) \left( \frac{1}{r} - \frac{1}{q^{\pm}} \right) + O(n^{-3/2}), & x < 0, \end{cases} \quad (16)$$

where  $r$  carries the sign of  $u_x - \tau$  and  $q^{\pm}$  carries the same sign as  $r$ .

Confidence limits follow by inversion of directed tails. Let  $t_L$  and  $t_U$  solve  $p_{\downarrow}(t_L) = \alpha/2$  and  $p_{\uparrow}(t_U) = \alpha/2$ . The mapping  $t \mapsto p_{\downarrow}(t)$  is monotone on  $(-\infty, \hat{q}_{\tau}]$  and  $t \mapsto p_{\uparrow}(t)$  on  $[\hat{q}_{\tau}, \infty)$  under (A2). A second-order coverage result is obtained by linearizing the composition  $t \mapsto F(t) \mapsto p$  at  $t = q_{\tau}$ . Write

$$z(t) = \frac{\sqrt{n}(F(t) - \tau)}{\sqrt{\tau(1-\tau)}}, \quad (17)$$

so that for the exact tail  $p^*(t) = \Phi(-z(t)) + O(n^{-1})$ . The sensitivity at  $q_{\tau}$  is

$$\frac{dp^*}{dt} \Big|_{t=q_{\tau}} = -\phi(0) \frac{\sqrt{n}f(q_{\tau})}{\sqrt{\tau(1-\tau)}}. \quad (18)$$

Combining (15) and (18) yields the following.

**Theorem 2** (Second-order coverage). *Assume (A1)-(A2). The equal-tailed  $(1 - \alpha)$  interval obtained by inverting the directed ESA tails satisfies*

$$\sup_{F \in \mathcal{F}} \left| \mathbb{P}_F \{q_\tau \in [t_L, t_U]\} - (1 - \alpha) \right| = O(n^{-1}), \quad (19)$$

*uniformly over families  $\mathcal{F}$  with  $f(q_\tau)$  bounded and bounded away from zero on a neighborhood of  $q_\tau$ . The constant is scale-modulated by  $f(q_\tau)^{-1}$  through (18).*

The self-normalization and the two-point structure imply robustness to heavy tails.

**Theorem 3** (Heavy-tail robustness). *Assume (A1) with  $f(q_\tau) > 0$ . Then the tail accuracy (15) and the coverage order (19) hold without any assumptions on the existence of moments of  $X$  or its tail index.*

The results extend to extreme quantiles with  $\tau = \tau_n$  provided the effective information  $n\tau_n(1 - \tau_n)$  diverges.

**Theorem 4** (Extreme quantiles). *Assume (A1)-(A3). Under the local regularity at  $q_{\tau_n}$ , the conclusions of Theorems 1-2 remain valid uniformly over compact  $x$ -sets. If a vanishing ridge  $Q_n \leftarrow Q_n + \epsilon_n$  is used with  $\epsilon_n \rightarrow 0$  (for instance  $\epsilon_n = cn^{-1/2}$ ), the orders are unchanged.*

When the sample contains ties or the underlying  $F$  assigns mass near  $q_\tau$ , directed tails can be evaluated using a mid-p modification or a Cornish-Fisher continuity shift. These corrections preserve the accuracy orders in Theorems 1-2 because they only regularize local discontinuities without changing the binomial mapping in Lemma 1.

## 4 Simulation study

This section outlines the simulation design for evaluating SNQESA against established confidence interval procedures for population quantiles. We begin by specifying the data-generating processes and computational details, then describe the benchmarking principles that guarantee equitable comparisons across methods, and conclude with definitions of the performance metrics appearing in subsequent tables.

Our simulation study draws independent samples  $(X_1, \dots, X_n)$  from five distributions chosen to challenge different aspects of quantile inference: standard normal, lognormal, Student's  $t$ , standard Cauchy, beta, exponential and the mixture  $0.5\mathcal{N}(-1, 1) + 0.5\mathcal{N}(1, 1)$ . For the normal, lognormal, and Student's  $t$  distributions, the target quantile  $q_\tau$  has known closed form. For the mixture distribution, we compute  $q_\tau$  via robust root-finding with automatic bracketing, falling back to Monte Carlo approximation if the bracketing fails to identify a sign change. The primary configuration uses  $n = 100$  and  $\tau = 0.95$ , with sensitivity analyses considering alternative values.

We implement SNQESA in two forms. The discrete version constructs equal-tailed and minimum-length intervals by inverting exact binomial tails for the count  $K = \sum_{i=1}^n \mathbf{1}\{X_i \leq t\}$ . The continuous version evaluates directed tails of the self-normalized statistic using constrained empirical saddlepoint approximation with Barndorff-Nielsen's  $r^*$  calibration. Near lattice boundaries, we stabilize computations with a continuity correction (Jeffreys by default) applied to the binomial tilt magnitude while preserving the uncorrected tilt direction. To prevent numerical singularities, we add a vanishing ridge  $\epsilon_n = cn^{-1/2}$  to  $Q_n$ , maintaining higher-order accuracy. When the constrained solver nears degeneracy, we revert to the algebraically equivalent one-parameter binomial tilt via the monotone mapping between  $T_n(t)$  and  $\bar{Y}_n(t)$ .

Competing methods include kernel-based, exact, bootstrap, subsampling, and linear-weight approaches, all at nominal level  $1 - \alpha = 0.95$ . Kernel-Wald intervals estimate  $f(q_\tau)$  using default kernel density estimation at the sample quantile, with a positivity constraint to stabilize delta-method standard errors. Exact order-statistic inversion uses the binomial distribution for  $K$ , mapping rank bounds to sample order statistics and treating  $n + 1$  as an infinite upper endpoint. Percentile and BCa bootstrap methods employ  $B = 1000$  resamples with type 8 sample quantiles; BCa uses standard jackknife estimates for bias and acceleration. The smoothed bootstrap incorporates normal noise with rule-of-thumb bandwidth selection. Harrell-Davis intervals combine HD estimation with percentile bootstrap, while Maritz-Jarrett intervals use HD weights for variance approximation with normal referencing. Subsampling uses without-replacement samples of size  $b \approx n^{0.7}$  and the pivot  $2\hat{q}_\tau - \hat{q}_{\tau,b}$ ;  $m$ -out-of- $n$  bootstrap draws with-replacement samples of size  $m \approx n^{0.7}$ . Hall-Sheather (medians) and Nyblom (general  $\tau$ ) intervals come from standard implementations. All methods process identical samples within replications to eliminate cross-method Monte Carlo variation.

Our evaluation adheres to three principles. First, intervals share common nominal levels and default tuning parameters. Second, all methods requiring point estimates use  $\hat{q}_\tau = \text{quantile}(X, \text{type} = 8)$ , isolating interval construction effects from estimation differences. Third, resampling methods employ identical  $B$  and shared random seeds within replications to minimize contrast variance.

Let  $q_\tau$  be the true quantile. For each procedure and replication, we record coverage  $\mathbf{1}\{L \leq q_\tau \leq U\}$ , interval length  $U - L$  (missing if infinite), failure indicators, and wall-clock time. Coverage standard errors use the binomial formula  $\sqrt{\hat{p}(1 - \hat{p})/R}$  with large, fixed  $R$ .

Two secondary metrics assess interval quality and point accuracy. The interval score

$$\text{IS}_\alpha(L, U; \theta) = (U - L) + \frac{2}{\alpha}(L - \theta)\mathbf{1}\{\theta < L\} + \frac{2}{\alpha}(\theta - U)\mathbf{1}\{\theta > U\},$$

where  $\theta = q_\tau$ , penalizes both width and miscoverage (smaller is better).

For each method, we report across replications: coverage with standard error, mean and median length, failure rate, mean time, and mean interval. All comparisons derive from common Monte Carlo samples, ensuring observed differences reflect methodological variations rather than simulation noise.

*Remark 1.* All simulations are implemented in **R**. Core functionality relies on base **R**, with `quantileCI` providing Hall–Sheather and Nyblom intervals, and `pbmcapply` enabling parallel replication on MacOS systems (serial execution on Windows). Random number generation is controlled via `set.seed` with derived seeds per replication to ensure reproducibility while maintaining alignment across methods. Computational timing uses `proc.time`. All implementation details follow the specifications outlined in the main text.

Table 1: Coverage and length across methods ( $\mathcal{N}(0, 1)$ ,  $\tau = 0.95$ ,  $n = 100$ ,  $\alpha = 0.05$ ).

Method	Cov.	$se_C$	$\bar{L}$	$\tilde{L}$	$\bar{t}$	$\bar{b}$	$\tilde{b}$	RMSE( $b$ )	$\bar{IS}$	$\tilde{IS}$
SNQESA	0.949	0.0151	0.6969	0.6696	0.0037	-0.0507	-0.0650	0.1886	0.8530	0.7037
WaldKDE	0.912	0.0127	0.7475	0.7323	0.0004	0.0038	-0.0007	0.1992	1.0308	0.7637
HDBoot	0.946	0.0101	0.7522	0.7333	0.0505	0.0274	0.0198	0.1763	0.8973	0.7585
PctBoot	0.950	0.0097	0.8157	0.7933	0.0536	0.0200	0.0147	0.1812	0.9998	0.8190
BCa	0.952	0.0096	0.8263	0.7901	0.0569	0.0520	0.0515	0.1940	0.9983	0.8234
SmBoot	0.974	0.0071	0.8421	0.8190	0.0605	0.1078	0.1007	0.2022	0.9002	0.8275
HS_Nyblom	0.960	0.0088	0.8880	0.8578	0.0046	0.0908	0.0919	0.2083	0.9879	0.8803
SNQESA <sub>min</sub>	0.960	0.0088	0.8895	0.8577	0.0005	0.0568	0.0493	0.1986	1.0235	0.8819
MaritzJar	0.956	0.0092	0.8971	0.8594	0.0001	0.0238	0.0187	0.1869	1.0305	0.8800
Subsample	0.960	0.0088	1.2372	1.2227	0.0512	-0.0124	-0.0211	0.3085	1.4089	1.2327
SNQESA <sub>disc</sub>	0.990	0.0044	1.2513	1.2303	0.0001	0.2265	0.2177	0.3209	1.2761	1.2303
Exact	0.990	0.0044	1.2513	1.2303	0.0001	0.2265	0.2177	0.3209	1.2761	1.2303
mOutOfn	0.994	0.0035	1.4144	1.4043	0.0509	0.0332	0.0288	0.1977	1.4232	1.4091

*Notes.* Cov. = coverage;  $se_C$  = standard error of coverage;  $\bar{L}$  /  $\tilde{L}$  = mean/median interval length;  $\bar{t}$  = mean time per replication (seconds);  $\bar{b}$  /  $\tilde{b}$  = mean/median center bias (interval center minus true  $q_\tau$ ); RMSE( $b$ ) = RMSE of center bias;  $\bar{IS}$  /  $\tilde{IS}$  = mean/median interval score.

Table 2: Coverage and length across methods (lognormal,  $\tau = 0.95$ ,  $n = 100$ ,  $\alpha = 0.05$ ).

Method	Cov.	$se_C$	$\bar{L}$	$\tilde{L}$	$\bar{t}$	$\bar{b}$	$\tilde{b}$	RMSE( $b$ )	$\bar{IS}$	$\tilde{IS}$
WaldKDE	0.452	0.0223	1.2265	1.2211	0.0005	0.1371	0.0133	1.1090	16.5260	3.9022
SNQESA	0.948	0.0151	3.6928	3.3092	0.0041	0.1897	0.0126	1.1579	5.0452	3.7639
SmBoot	0.946	0.0101	4.6384	4.2682	0.0599	0.7582	0.5941	1.4815	5.5026	4.4563
HDBoot	0.946	0.0101	4.6960	4.2397	0.0515	0.9486	0.7487	1.6157	5.3614	4.3770
PctBoot	0.948	0.0099	4.7316	4.3443	0.0579	0.7529	0.5671	1.4900	5.6254	4.5737
BCa	0.952	0.0096	4.9337	4.4034	0.0576	0.9497	0.7586	1.6846	5.7994	4.5753
SNQESA <sub>min</sub>	0.960	0.0088	5.3304	4.8681	0.0006	1.0267	0.8598	1.7666	6.0126	4.9922
MaritzJar	0.960	0.0088	5.5307	5.0084	0.0001	0.3895	0.2441	1.1590	6.1555	5.1781

Method	<i>Cov.</i>	<i>se<sub>C</sub></i>	$\bar{L}$	$\tilde{L}$	$\bar{t}$	$\bar{b}$	$\tilde{b}$	RMSE( $b$ )	$\bar{IS}$	$\tilde{IS}$
HS_Nyblom	0.966	0.0081	5.6363	5.1350	0.0050	1.3297	1.1206	2.0073	6.1081	5.1689
Subsample	0.924	0.0119	7.6573	6.9848	0.0517	-1.2922	-1.2650	2.3541	8.9299	7.3877
mOutOfn	0.994	0.0035	9.0206	8.1657	0.0528	2.0365	1.5974	3.0644	9.0621	8.1907
SNQESA <sub>disc</sub>	0.990	0.0044	9.6177	8.3085	0.0001	3.1522	2.4550	4.2992	9.7532	8.3085
Exact	0.990	0.0044	9.6177	8.3085	0.0001	3.1522	2.4550	4.2992	9.7532	8.3085

Notes. *Cov.* = coverage; *se<sub>C</sub>* = standard error of coverage;  $\bar{L}$  /  $\tilde{L}$  = mean/median interval length;  $\bar{t}$  = mean time per replication (seconds);  $\bar{b}$  /  $\tilde{b}$  = mean/median center bias (interval center minus true  $q_\tau$ ); RMSE( $b$ ) = RMSE of center bias;  $\bar{IS}$  /  $\tilde{IS}$  = mean/median interval score.

Table 3: Coverage and length across methods ( $t(2)$ ,  $\tau = 0.95$ ,  $n = 100$ ,  $\alpha = 0.05$ ).

Method	<i>Cov.</i>	<i>se<sub>C</sub></i>	$\bar{L}$	$\tilde{L}$	$\bar{t}$	$\bar{b}$	$\tilde{b}$	RMSE( $b$ )	$\bar{IS}$	$\tilde{IS}$
WaldKDE	0.618	0.0217	1.3382	1.3450	0.0005	0.1319	-0.0438	0.8590	9.0513	1.5340
SNQESA	0.954	0.0148	2.5814	2.2650	0.0041	0.1895	0.0791	0.9097	3.1274	2.1138
SmBoot	0.958	0.0090	3.4388	2.9614	0.0601	0.7545	0.5496	1.3894	3.9113	3.0551
PctBoot	0.944	0.0103	3.5361	3.0817	0.0572	0.7010	0.4696	1.3774	4.2611	3.2064
BCa	0.942	0.0105	3.7549	3.1491	0.0596	0.8788	0.6259	1.6111	4.5221	3.2618
HDBoot	0.944	0.0103	4.0841	3.2550	0.0544	1.1257	0.7128	2.4905	4.8627	3.3099
SNQESA <sub>min</sub>	0.952	0.0096	4.0998	3.4367	0.0006	0.9608	0.6333	1.7202	4.7765	3.5634
HS_Nyblom	0.944	0.0103	4.6754	3.7850	0.0096	1.3617	0.9349	2.3483	5.2991	3.9260
MaritzJar	0.964	0.0083	4.6775	3.5809	0.0001	0.3461	0.1840	0.9409	5.0684	3.8353
Subsample	0.924	0.0119	7.0561	5.2088	0.0543	-1.7817	-1.0627	4.9366	7.8043	5.6678
mOutOfn	0.992	0.0040	9.4002	6.0010	0.0520	3.0852	1.4242	10.8490	9.4564	6.0652
SNQESA <sub>disc</sub>	0.980	0.0063	10.5304	6.5161	0.0001	4.1641	2.1699	11.6343	10.7635	6.6070
Exact	0.980	0.0063	10.5304	6.5161	0.0001	4.1641	2.1699	11.6343	10.7635	6.6070

Notes. *Cov.* = coverage; *se<sub>C</sub>* = standard error of coverage;  $\bar{L}$  /  $\tilde{L}$  = mean/median interval length;  $\bar{t}$  = mean time per replication (seconds);  $\bar{b}$  /  $\tilde{b}$  = mean/median center bias (interval center minus true  $q_\tau$ ); RMSE( $b$ ) = RMSE of center bias;  $\bar{IS}$  /  $\tilde{IS}$  = mean/median interval score.

Table 4: Coverage and length across methods (Cauchy,  $\tau = 0.5$ ,  $n = 50$ ,  $\alpha = 0.05$ ).

Method	<i>Cov.</i>	<i>se<sub>C</sub></i>	$\bar{L}$	$\tilde{L}$	$\bar{t}$	$\bar{b}$	$\tilde{b}$	RMSE( $b$ )	$\bar{IS}$	$\tilde{IS}$
SNQESA	0.951	0.0068	1.7832	1.7365	0.0099	-0.0293	-0.0325	0.4551	2.0652	1.7758
HDBoot	0.956	0.0065	1.8026	1.7677	0.0400	-0.0239	-0.0367	0.4478	2.1218	1.8003
BCa	0.952	0.0068	1.8434	1.8201	0.0542	-0.0865	-0.0733	0.4689	2.1742	1.8454
PctBoot	0.961	0.0061	1.8536	1.8136	0.0513	-0.0270	-0.0306	0.4547	2.1440	1.8568
SNQESA <sub>min</sub>	0.956	0.0065	1.8610	1.8339	0.0006	-0.0293	-0.0324	0.4591	2.1443	1.8565
HS_Nyblom	0.965	0.0058	1.8846	1.8474	0.0028	-0.0273	-0.0313	0.4559	2.1402	1.8736
MaritzJar	0.969	0.0055	1.9296	1.8835	0.0001	-0.0216	-0.0174	0.4240	2.1192	1.9137
SNQESA <sub>disc</sub>	0.976	0.0048	2.0921	2.0411	0.0001	-0.0232	-0.0217	0.4664	2.2554	2.0628
Exact	0.976	0.0048	2.0921	2.0411	0.0001	-0.0232	-0.0217	0.4664	2.2554	2.0628
SmBoot	0.986	0.0037	2.2249	2.1822	0.0561	-0.0279	-0.0318	0.4658	2.3118	2.1949
WaldKDE	0.984	0.0040	2.2384	2.1998	0.0004	-0.0161	-0.0218	0.4358	2.3292	2.2175
Subsample	0.978	0.0046	2.9079	2.8484	0.0517	-0.0073	0.0108	0.5742	3.0444	2.8821
mOutOfn	1.000	0.0000	3.7128	3.6017	0.0510	-0.0340	-0.0201	0.5966	3.7128	3.6017

Notes. *Cov.* = coverage; *se<sub>C</sub>* = standard error of coverage;  $\bar{L}$  /  $\tilde{L}$  = mean/median interval length;  $\bar{t}$  = mean time per replication (seconds);  $\bar{b}$  /  $\tilde{b}$  = mean/median center bias (interval center minus true  $q_\tau$ ); RMSE( $b$ ) = RMSE of center bias;  $\bar{IS}$  /  $\tilde{IS}$  = mean/median interval score.

Table 5: Coverage and length across methods (Cauchy,  $\tau = 0.95, n = 100, \alpha = 0.05$ ).

Method	$Cov.$	$se_C$	$\bar{L}$	$\tilde{L}$	$\bar{t}$	$\bar{b}$	$\tilde{b}$	RMSE( $b$ )	$\bar{IS}$	$\tilde{IS}$
WaldKDE	0.254	0.0195	3.3112	3.3236	0.0004	1.8095	0.0407	7.6848	142.52	70.537
SNQESA	0.951	0.0152	23.234	16.922	0.0049	5.0495	1.9573	14.0073	33.732	20.282
SmBoot	0.950	0.0097	41.002	26.285	0.0641	14.338	6.9981	27.1663	45.237	28.121
PctBoot	0.950	0.0097	41.327	26.551	0.0590	14.283	6.9146	27.1304	45.800	28.288
BCa	0.948	0.0099	45.723	28.523	0.0653	16.862	8.2889	31.5017	50.639	30.030
SNQESA <sub>min</sub>	0.960	0.0088	51.337	32.214	0.0005	19.123	9.5784	35.7201	55.081	34.071
HS_Nyblom	0.950	0.0097	104.74	40.255	0.0050	46.482	14.442	200.982	108.76	41.580
HDBoot	0.934	0.0111	125.27	35.898	0.0547	57.436	12.531	320.233	133.00	37.740
MaritzJar	0.978	0.0066	143.57	38.914	0.0001	6.7266	3.1146	17.5490	146.47	39.903
Subsample	0.870	0.0150	252.68	63.407	0.0564	-114.42	-20.654	714.421	262.86	69.066
mOutOfn	0.994	0.0035	329.61	78.395	0.0580	155.93	29.975	756.787	330.08	79.004
SNQESA <sub>disc</sub>	0.980	0.0063	550.36	86.643	0.0001	268.61	36.594	1785.86	551.95	86.726
Exact	0.980	0.0063	550.36	86.643	0.0001	268.61	36.594	1785.86	551.95	86.726

Notes.  $Cov.$  = coverage;  $se_C$  = standard error of coverage;  $\bar{L}$  /  $\tilde{L}$  = mean/median interval length;  $\bar{t}$  = mean time per replication (seconds);  $\bar{b}$  /  $\tilde{b}$  = mean/median center bias (interval center minus true  $q_\tau$ ); RMSE( $b$ ) = RMSE of center bias;  $\bar{IS}$  /  $\tilde{IS}$  = mean/median interval score.

 Table 6: Coverage and length across methods ( $0.5\mathcal{N}(-1, 1) + 0.5\mathcal{N}(1, 1)$ ,  $\tau = 0.95, n = 100, \alpha = 0.05$ ).

Method	$Cov.$	$se_C$	$\bar{L}$	$\tilde{L}$	$\bar{t}$	$\bar{b}$	$\tilde{b}$	RMSE( $b$ )	$\bar{IS}$	$\tilde{IS}$
SNQESA	0.944	0.0155	0.8047	0.7750	0.0043	-0.0700	-0.0610	0.2269	1.5126	0.8679
HDBoot	0.918	0.0123	0.8611	0.8392	0.0567	0.0195	0.0259	0.2145	1.1241	0.8859
WaldKDE	0.914	0.0125	0.9081	0.8717	0.0005	0.0074	0.0056	0.2406	1.2208	0.9070
PctBoot	0.928	0.0116	0.9307	0.8998	0.0624	0.0104	0.0197	0.2223	1.2256	0.9476
BCa	0.916	0.0124	0.9375	0.9099	0.0646	0.0485	0.0654	0.2358	1.2366	0.9592
HS_Nyblom	0.932	0.0113	1.0034	0.9722	0.0078	0.0930	0.0971	0.2518	1.2104	1.0210
SNQESA <sub>min</sub>	0.938	0.0108	1.0124	0.9836	0.0009	0.0537	0.0603	0.2427	1.2550	1.0207
MaritzJar	0.934	0.0111	1.0167	0.9624	0.0001	0.0279	0.0256	0.2256	1.2227	1.0238
SmBoot	0.968	0.0079	1.0350	1.0111	0.0659	0.1643	0.1619	0.2671	1.1213	1.0174
SNQESA <sub>disc</sub>	0.980	0.0063	1.4288	1.3953	0.0003	0.2421	0.2455	0.3637	1.4680	1.4061
Exact	0.980	0.0063	1.4288	1.3953	0.0001	0.2421	0.2455	0.3637	1.4680	1.4061
Subsample	0.950	0.0097	1.4436	1.4259	0.0563	0.0235	0.0195	0.3693	1.6863	1.4434
mOutOfn	0.988	0.0049	1.6642	1.6396	0.0568	-0.0008	0.0005	0.2424	1.6967	1.6537

Notes.  $Cov.$  = coverage;  $se_C$  = standard error of coverage;  $\bar{L}$  /  $\tilde{L}$  = mean/median interval length;  $\bar{t}$  = mean time per replication (seconds);  $\bar{b}$  /  $\tilde{b}$  = mean/median center bias (interval center minus true  $q_\tau$ ); RMSE( $b$ ) = RMSE of center bias;  $\bar{IS}$  /  $\tilde{IS}$  = mean/median interval score.

 Table 7: Coverage and length across methods (Beta,  $\tau = 0.95, n = 100, \alpha = 0.05$ ).

Method	$Cov.$	$se_C$	$\bar{L}$	$\tilde{L}$	$\bar{t}$	$\bar{b}$	$\tilde{b}$	RMSE( $b$ )	$\bar{IS}$	$\tilde{IS}$
SNQESA	0.951	0.0106	0.0233	0.0208	0.0081	-0.0083	-0.0067	0.0121	0.0444	0.0224
HS_Nyblom	0.945	0.0072	0.0253	0.0227	0.0035	-0.0078	-0.0063	0.0114	0.0317	0.0235
SNQESA <sub>min</sub>	0.948	0.0070	0.0254	0.0228	0.0006	-0.0074	-0.0059	0.0111	0.0316	0.0235
BCa	0.930	0.0081	0.0258	0.0233	0.0579	-0.0084	-0.0068	0.0119	0.0339	0.0239
HDBoot	0.891	0.0099	0.0281	0.0253	0.0501	-0.0109	-0.0092	0.0141	0.0439	0.0258
PctBoot	0.930	0.0081	0.0285	0.0256	0.0538	-0.0100	-0.0081	0.0135	0.0381	0.0261
MaritzJar	0.970	0.0054	0.0304	0.0272	0.0001	-0.0035	-0.0018	0.0078	0.0337	0.0279
SNQESA <sub>disc</sub>	0.984	0.0040	0.0309	0.0277	0.0001	-0.0098	-0.0081	0.0131	0.0320	0.0278

Method	$Cov.$	$se_C$	$\bar{L}$	$\tilde{L}$	$\bar{t}$	$\bar{b}$	$\tilde{b}$	$RMSE(b)$	$\bar{IS}$	$\tilde{IS}$
Exact	0.984	0.0040	0.0309	0.0277	0.0001	-0.0098	-0.0081	0.0131	0.0320	0.0278
Subsample	0.767	0.0134	0.0639	0.0594	0.0540	0.0229	0.0222	0.0260	0.0859	0.0718
mOutOfn	0.990	0.0031	0.0786	0.0738	0.0516	-0.0339	-0.0314	0.0372	0.0801	0.0740
WaldKDE	1.000	0.0000	0.1061	0.1042	0.0004	-0.0020	0.0000	0.0073	0.1061	0.1042
SmBoot	0.553	0.0157	0.1528	0.1525	0.0582	0.0715	0.0727	0.0744	0.4234	0.1670

Notes.  $Cov.$  = coverage;  $se_C$  = standard error of coverage;  $\bar{L}$  /  $\tilde{L}$  = mean/median interval length;  $\bar{t}$  = mean time per replication (seconds);  $\bar{b}$  /  $\tilde{b}$  = mean/median center bias (interval center minus true  $q_\tau$ );  $RMSE(b)$  = RMSE of center bias;  $\bar{IS}$  /  $\tilde{IS}$  = mean/median interval score.

Table 8: Coverage and length across methods (Exp,  $\tau = 0.95$ ,  $n = 100$ ,  $\alpha = 0.05$ ).

Method	$Cov.$	$se_C$	$\bar{L}$	$\tilde{L}$	$\bar{t}$	$\bar{b}$	$\tilde{b}$	$RMSE(b)$	$\bar{IS}$	$\tilde{IS}$
WaldKDE	0.698	0.0145	0.9107	0.9007	0.0004	0.0776	0.0718	0.4528	3.9690	0.9899
SNQESA	0.947	0.0107	1.4026	1.3149	0.0089	0.0672	0.0416	0.4348	1.8106	1.4718
HDBoot	0.944	0.0073	1.6895	1.6107	0.0502	0.2221	0.2019	0.4877	2.0255	1.6768
SmBoot	0.964	0.0059	1.7623	1.6557	0.0594	0.2170	0.1832	0.4887	2.0046	1.7041
PctBoot	0.948	0.0070	1.8040	1.7008	0.0540	0.1890	0.1542	0.4896	2.1533	1.7674
BCa	0.942	0.0074	1.8467	1.7312	0.0569	0.2657	0.2295	0.5485	2.1901	1.7945
SNQESA <sub>min</sub>	0.952	0.0068	1.9903	1.8731	0.0005	0.2754	0.2325	0.5639	2.2785	1.9506
HS_Nyblom	0.956	0.0065	2.0197	1.9056	0.0035	0.3657	0.3312	0.6168	2.2935	1.9659
MaritzJar	0.958	0.0063	2.0291	1.8898	0.0001	0.1438	0.1223	0.4485	2.2597	1.9392
Subsample	0.938	0.0076	2.7289	2.5895	0.0519	-0.1549	-0.1587	0.7166	3.1690	2.7031
SNQESA <sub>disc</sub>	0.980	0.0044	3.0250	2.7482	0.0001	0.7777	0.6832	1.0571	3.1085	2.7942
Exact	0.980	0.0044	3.0250	2.7482	0.0000	0.7777	0.6832	1.0571	3.1085	2.7942
mOutOfn	0.988	0.0034	3.1482	2.9348	0.0499	0.4082	0.3168	0.7462	3.2159	2.9756

Notes.  $Cov.$  = coverage;  $se_C$  = standard error of coverage;  $\bar{L}$  /  $\tilde{L}$  = mean/median interval length;  $\bar{t}$  = mean time per replication (seconds);  $\bar{b}$  /  $\tilde{b}$  = mean/median center bias (interval center minus true  $q_\tau$ );  $RMSE(b)$  = RMSE of center bias;  $\bar{IS}$  /  $\tilde{IS}$  = mean/median interval score.

We first consider the Gaussian design. In Table 1, our continuous SNQESA attains coverage 0.949, essentially on target, while delivering the shortest mean length among all well-calibrated procedures (0.697). The interval score is the lowest in the panel, and the center bias is small and slightly negative. Resampling competitors reach nominal coverage but are uniformly longer (for example BCa at 0.826 and Percentile at 0.816), whereas WaldKDE undercovers at 0.912. The discrete inversion variants, including Exact and SNQESA<sub>disc</sub>, are conservative at 0.990 and come with substantially larger lengths around 1.25. Runtime-wise, SNQESA is orders of magnitude faster than bootstrap-based methods and remains comparable to lightweight closed-form baselines.

Under strong right-skewness (lognormal), Table 2 highlights a pronounced failure of WaldKDE (coverage 0.452). By contrast, SNQESA remains well calibrated (0.948) and attains shorter intervals than all other nominal competitors; it also achieves the best interval score in this panel. Percentile and BCa reach the nominal level but require visibly longer intervals, reflecting their difficulty in the upper tail. As in the Gaussian case, discrete inversions are accurate but very conservative in length.

Heavy symmetric tails are examined with the  $t(2)$  design in Table 3. SNQESA maintains nominal coverage (0.954) with substantially shorter intervals than all resampling alternatives, while WaldKDE again undercovers (0.618). Maritz-Jarrett yields slightly higher coverage but only at the cost of much longer intervals and a worse interval score; Exact-type procedures remain the most conservative.

When focusing on the Cauchy median (Table 4), most robust methods achieve near-nominal coverage. Here SNQESA provides the shortest intervals among the well-calibrated group (mean length 1.783) and the best or near-best interval scores, with very small center bias. Discrete inversions are mildly conservative and longer, and m-out-of-n exhibits perfect but excessively conservative coverage with correspondingly large length.

The extreme-tail Cauchy experiment at  $\tau = 0.95$  (Table 5) is the most challenging scenario. WaldKDE collapses with 0.254 coverage. SNQESA achieves nominal coverage (0.951) with dramatically shorter

intervals than all other calibrated competitors (mean length about 23, versus 41-46 for bootstrap methods and over 100 for HS-Nyblom). Interval scores mirror this advantage. Maritz-Jarrett attains high coverage but only by inflating length to well beyond 100, and discrete inversions are accurate yet extremely wide.

For the bimodal mixture (Table 6), nearly all methods exhibit mild undercoverage, a known difficulty when the density dips near the target quantile. SNQESA is slightly below nominal (0.944) while producing the shortest intervals in the well-performing group. Smoothed bootstrap attains higher coverage (0.968) with moderate lengths and competitive scores, illustrating that smoothing can help in multimodal settings; the price is a larger positive center bias. Discrete inversions again deliver excellent coverage but at a notable cost in length.

Bounded-support behavior is assessed with the Beta design in Table 7. SNQESA is on target (0.951) and attains the shortest intervals among the nominal methods, with the best overall interval scores and small bias. Several bootstrap variants undercover here, and WaldKDE is perfectly calibrated only by being markedly conservative in length; smoothed bootstrap severely undercovers near the boundary.

Finally, with the exponential design (Table 8), SNQESA stays near nominal (0.947) and again provides the shortest intervals among well-calibrated competitors, delivering favorable interval scores and modest bias. Bootstrap procedures reach the target but require longer intervals, while WaldKDE undercovers.

Across all designs, we observe a consistent pattern. First, continuous SNQESA tracks the nominal level closely in light-tailed, heavy-tailed, and skewed cases and does so with some of the shortest lengths and best interval scores. Second, purely discrete inversions and m-out-of-n procedures provide coverage insurance at the expense of substantially larger intervals. Third, WaldKDE is fast but unreliable under tail complexity and boundary effects, while resampling methods are slower and tend to be conservative in difficult tails. The only systematic tension for SNQESA appears under pronounced multimodality, where mild undercoverage can arise alongside very short intervals; in such cases, a more conservative tail split or ridge choice can trade a small increase in length for improved calibration. Overall, the results support SNQESA as a uniformly competitive default that balances calibration, efficiency, and speed across a wide spectrum of distributions and quantile levels.

## 5 Empirical analysis

This section evaluates the proposed SNQESA inference in a one-day market risk setting. Let  $r_t$  denote daily log-returns on the S&P 500 index, obtained from the Federal Reserve Bank of St. Louis (FRED). For each business day  $t$ , a one-step-ahead left-tail VaR forecast at level  $\tau = 0.99$  is computed from a rolling window of  $m = 250$  past observations,

$$\text{VaR}_{t+1|t}^{(\tau)} = \inf\{v : \mathbb{P}(r_{t+1} \leq v | \mathcal{F}_t) \geq \tau\}.$$

Define exceedance indicators

$$I_{t+1} = \mathbf{1}\{r_{t+1} \leq \text{VaR}_{t+1|t}^{(\tau)}\},$$

with nominal exceedance probability  $\pi = 1 - \tau = 0.01$ . For Historical Simulation (HS) and Filtered Historical Simulation (FHS),  $(1 - \alpha)$  confidence intervals for  $\text{VaR}_{t+1|t}^{(\tau)}$  are constructed via SNQESA at each  $t$ . As benchmarks we include Delta-Normal, Monte Carlo with Student- $t$  innovations (MCt), peaks-over-threshold extreme value methods (EVT), quantile regression (QR), and GARCH(1,1); their VaR intervals are obtained by bootstrap. All procedures use the same rolling window and return series.

Backtesting follows the likelihood-ratio (LR) framework. Unconditional coverage (Kupiec POF) tests  $H_0 : \mathbb{P}(I_{t+1} = 1) = \pi$ . Writing  $N$  for the number of forecasts and  $n$  for the number of exceedances (Kupiec, 1995; Christoffersen, 1998),  $\hat{\pi} = n/N$ , the LR statistic is

$$\text{LR}_{\text{POF}} = -2 \left[ \log\{(1 - \pi)^{N-n} \pi^n\} - \log\{(1 - \hat{\pi})^{N-n} \hat{\pi}^n\} \right] \stackrel{H_0}{\sim} \chi_1^2. \quad (20)$$

Independence (Christoffersen IND) tests first-order Markov clustering in the hit sequence. Let  $n_{ij}$  be the number of transitions  $I_t = i \rightarrow I_{t+1} = j$ ,  $i, j \in \{0, 1\}$ , with  $\hat{p}_{01} = n_{01}/(n_{00} + n_{01})$  and  $\hat{p}_{11} = n_{11}/(n_{10} + n_{11})$ . Under independence the common conditional exceedance probability equals  $\hat{p} = \hat{\pi}$ , and

$$\text{LR}_{\text{IND}} = -2 \left[ \log\{(1 - \hat{p})^{n_{00}+n_{10}} \hat{p}^{n_{01}+n_{11}}\} - \log\{(1 - \hat{p}_{01})^{n_{00}} \hat{p}_{01}^{n_{01}} (1 - \hat{p}_{11})^{n_{10}} \hat{p}_{11}^{n_{11}}\} \right] \sim \chi_1^2. \quad (21)$$

Conditional coverage combines the two

$$\text{LR}_{\text{CC}} = \text{LR}_{\text{POF}} + \text{LR}_{\text{IND}} \sim \chi_2^2. \quad (22)$$

For interpretability we also report the empirical exceedance rate  $\hat{\pi}$  and the Basel traffic-light classification computed on non-overlapping windows of length  $m = 250$ ; for  $\tau = 0.99$  the green, yellow, and red zones correspond to at most 4 exceedances, 5-9 exceedances, and at least 10 exceedances, respectively.

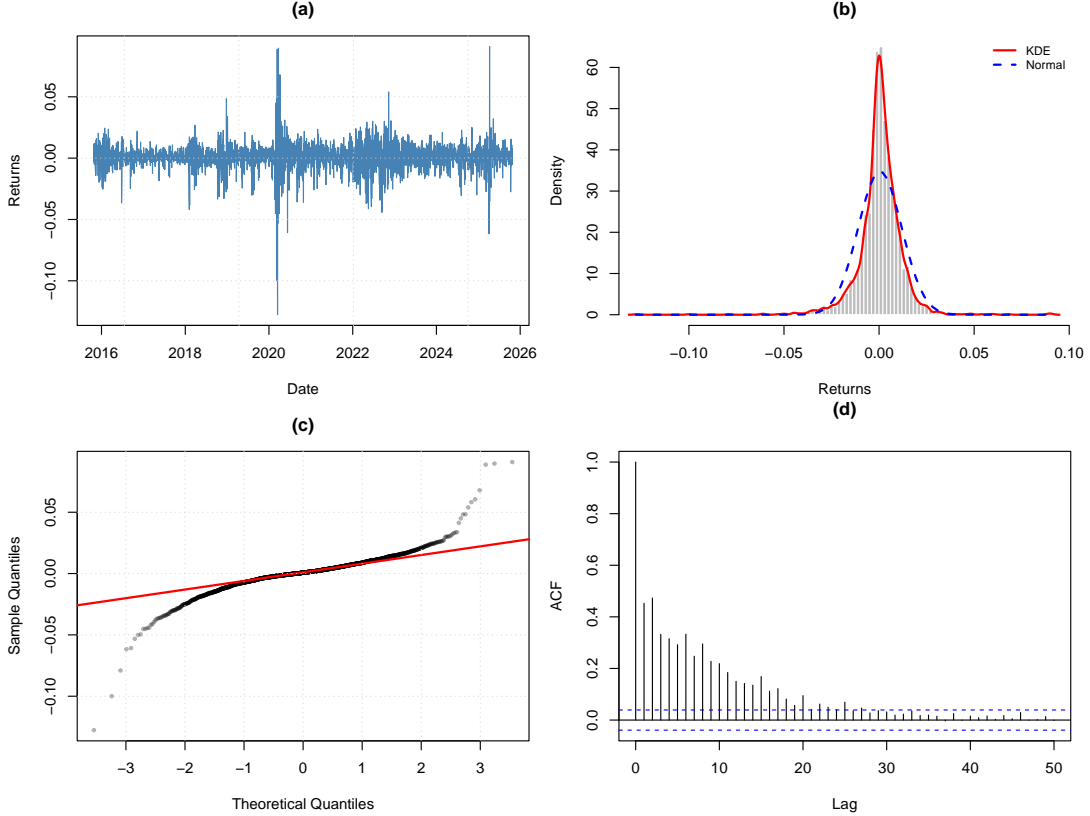


Figure 1: Daily log-returns (a) series; (b) histogram with KDE and normal; (c) normal Q-Q; (d) squared-returns ACF.

Table 9: Backtesting performance across VaR models

Method	PoF( $p$ -value)	$\pi$ (%)	IND( $p$ -value)	CC( $p$ -value)	green(%)	yellow(%)	red(%)
FHS	0.0061(0.9379)	1.016	0(1)	0.0064(0.0996)	89.72	10.27	0.00
HS	5.8534(0.0155)	1.546	0(1)	5.8645(0.0532)	52.85	39.27	8.63
MCT	0.0822(0.7744)	1.060	0(1)	0.0834(0.9591)	79.94	20.06	0.00
QR	4.2053(0.4029)	1.458	0(1)	4.2146(0.1215)	57.24	37.24	8.55
EVT	10.963(0.0929)	1.767	0(1)	10.979(0.1302)	50.19	41.16	8.63
GARCH	30.073(0.0416)	2.349	0(1)	30.100(0.2909)	30.37	64.79	4.87
EWHS	21.710(0.0000)	0.021	0(1)	21.733(0.0001)	40.39	51.21	8.39

Notes:  $\pi = 1 - \tau$ . PoF, IND, CC denote the LR statistics and  $p$ -values in (20), (21), and (22).

Table 9 indicates that FHS combined with SNQESA attains an empirical exceedance rate  $\hat{\pi} = 1.016\%$  close to the nominal level, with a very high POF  $p$ -value (0.9379). In contrast, HS exhibits a statistically significant deviation (POF  $p$ -value 0.0155,  $\hat{\pi} = 1.546\%$ ). All models show no detectable clustering in the hit process at the daily frequency (IND  $p$ -values near 1). Conditional coverage follows the same pattern, with FHS acceptable and HS borderline at the 5% level. The Basel classification places FHS in the green region in the vast majority of rolling years, with no red periods, whereas HS, QR, and EVT have non-negligible red shares.

Figure 2 complements Tables 10 and 9. Models reporting the narrowest intervals—Delta-Normal and GARCH—also display the largest deviations from nominal coverage (Table 9), indicating over-confidence in the left tail. In contrast, FHS delivers moderate interval widths (Table 10) together with near-nominal

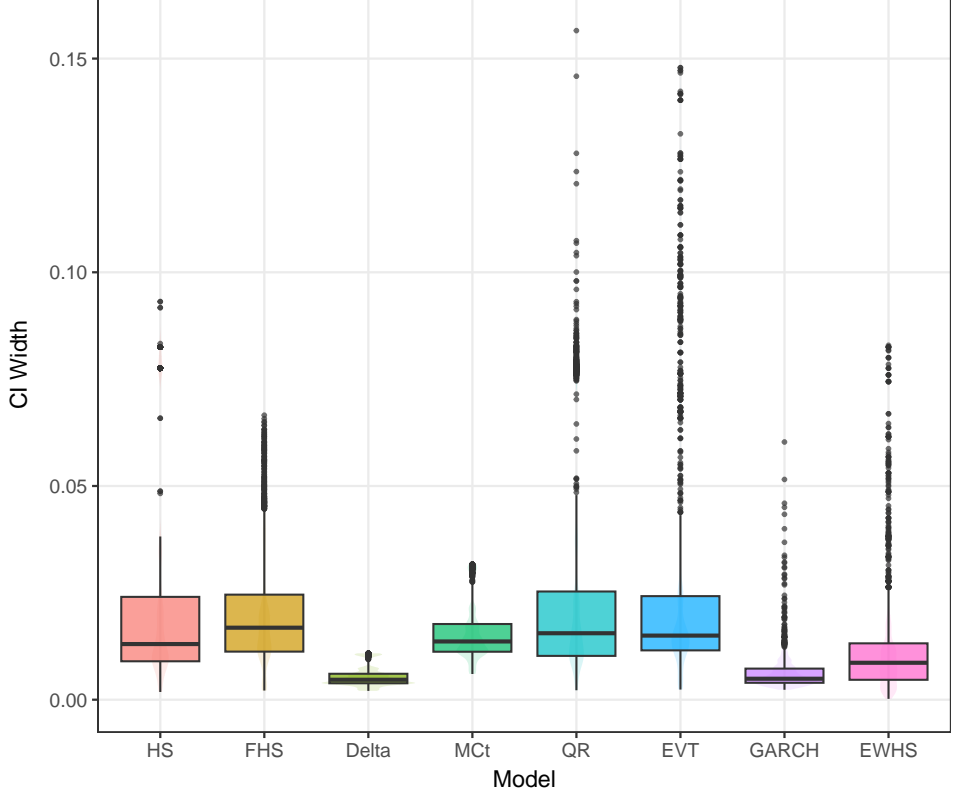


Figure 2: Distribution of VaR interval widths across models.

unconditional coverage ( $POF = 0.94$ ), suggesting that its uncertainty quantification is commensurate with forecast risk. MCt and QR/EVT exhibit wider and more dispersed widths, consistent with their heavier-tailed innovations or threshold uncertainty. The EWHS lies between HS and FHS, its slightly wider distribution relative to HS mirrors stronger responsiveness to scale shifts.

Table 10: Confidence-interval characteristics for VaR models

Method	$\bar{W}$	$sew$	$\tilde{W}$	$W_{\min}$	$W_{\max}$	$\bar{t}$ (s)
FHS (SNQESA)	0.02023	0.01388	0.01684	0.00214	0.06656	1.15
HS (SNQESA)	0.02186	0.02190	0.01301	0.00180	0.09314	1.12
MCt (Bootstrap)	0.02468	0.02625	0.01291	0.00551	0.03341	65.31
QR (Bootstrap)	0.02405	0.02250	0.01553	0.00226	0.14794	200.96
EVT (Bootstrap)	0.02252	0.02354	0.01426	0.00210	0.13279	86.39
GARCH (Bootstrap)	0.00578	0.00393	0.00468	0.00208	0.06081	814.3
EWHS (Bootstrap)	0.01191	0.01266	0.00864	0.00021	0.08292	95.712

*Notes:* HS and FHS intervals are constructed by SNQESA; others by bootstrap.  $W$ (Width) metrics correspond to nominal 95% VaR intervals.

Table 10 compares interval width and computational time. SNQESA produces shorter average intervals for HS and FHS than the bootstrap-based benchmarks (MCt, QR, EVT) at a fraction of the computational cost. Although the GARCH intervals are the narrowest, the unconditional coverage results in Table 9 caution against interpreting small absolute widths as genuine efficiency when model uncertainty may be underestimated.

Table 11: Stability metrics for VaR forecast paths

Method	VaR Volatility	Change Volatility	Max Drawdown	Turning Ratio	Stability
FHS	0.02681	0.00172	0.17522	0.37593	25.43
HS	0.01868	0.00090	0.06735	0.06191	140.95
MCt	0.01537	0.00041	0.05108	0.42857	23.10
QR	0.01898	0.00162	0.09316	0.45997	21.00
EVT	0.01747	0.00070	0.06941	0.61565	16.05
GARCH	0.01556	0.00466	0.21816	0.47914	19.01
EWHS	0.01685	0.00165	0.10949	0.05039	149.46

*Notes:* VaR Volatility is the standard deviation of  $\{\text{VaR}_t^{(\tau)}\}$ ; Change Volatility is the standard deviation of  $\Delta\text{VaR}_t = \text{VaR}_t^{(\tau)} - \text{VaR}_{t-1}^{(\tau)}$ ; Turning Ratio is the fraction of sign changes in  $\Delta\text{VaR}_t$ ; Stability is  $1/(\text{Change Volatility} + 0.1 \times \text{Turning Ratio})$ .

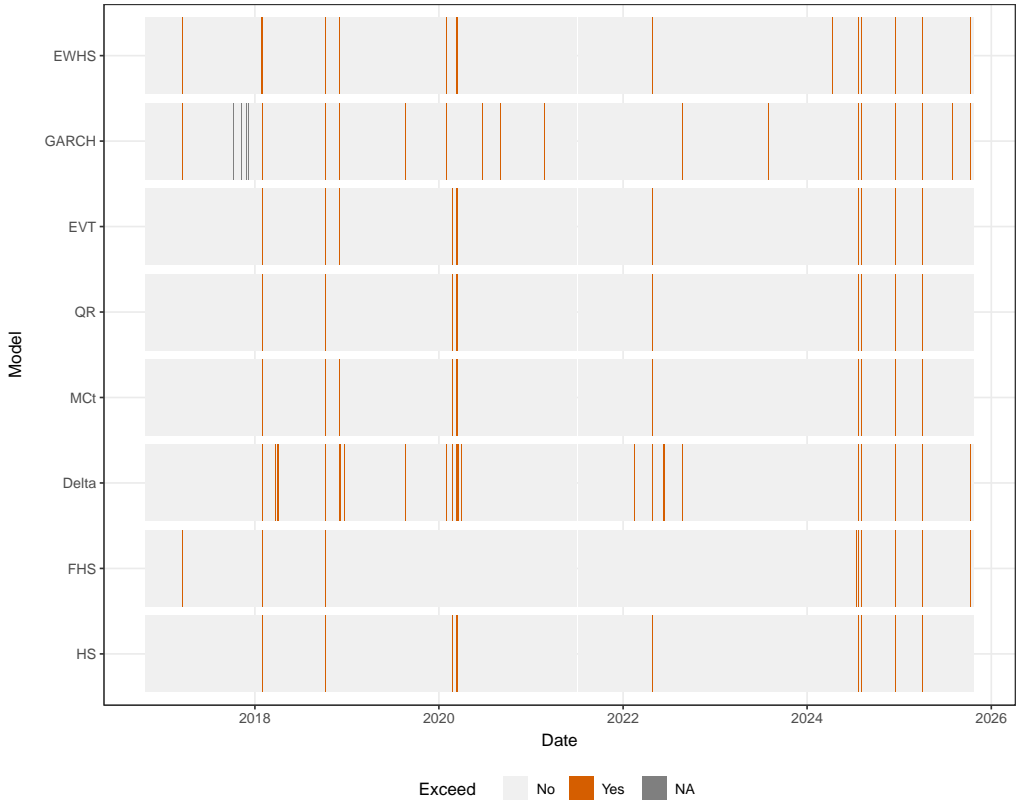


Figure 3: Exceedance heatmap ( $I_{t+1} = \mathbf{1}\{r_{t+1} \leq \text{VaR}_{t+1|t}^{0.99}\}$ )

Figure 3 visualizes the timing of VaR violations across models. Violations cluster around the 2020 pandemic crash and the 2022 tightening episode, indicating regime shifts rather than idiosyncratic noise. Models differ markedly in how often they breach during these stress windows: Delta-Normal and GARCH display the densest stripes, whereas FHS and MCt are comparatively sparse. This visual ranking matches the unconditional coverage results in Table 9: FHS attains an empirical exceedance rate close to the nominal 1% ( $\hat{\pi} = 1.016\%$ ), while Delta, QR, EVT and especially GARCH overshoot the nominal level. EWHS (exponentially-weighted HS) behaves similarly to FHS but reacts more to turning points, which is consistent with its recency weights.

The heatmap also aligns with our interval diagnostics. Models with the densest violation stripes (Delta, GARCH) are those reporting the narrowest VaR intervals in Table 10, suggesting underestimation of tail uncertainty. Conversely, FHS and MCt combine moderate interval width with fewer breaches. Conditional on a breach, the lollipop plots of exceedance severity show higher tails for Delta/GARCH, reinforcing the caution that narrower intervals do not necessarily imply better efficiency when model risk is material.

Table 11 assesses temporal regularity of the forecast sequences. FHS exhibits higher change volatility than HS, indicating greater responsiveness to shifts in conditional scale, while its turning ratio and drawdown do not suggest excessive oscillation. HS displays very low change volatility but, combined with its unconditional coverage deviation, this points to sluggish adjustment to distributional changes.

Table 12: Extreme-event performance (best VaR models, 2018–2023)

Period	Method	Fail	Gap	Ratio	Score	K
2018 Q4 Drawdown	QR	0.1	-0.0081	0.983	0.925	10
2018 Volmageddon	FHS	0.2	-0.0336	0.937	0.841	10
2020 COVID Crash	FHS	0.2	-0.0557	0.983	0.855	10
2020 US Election Vol.	HS	0.0	-0.0837	1.000	1.000	10
2022 Fed Tightening Bear	FHS	0.1	-0.0057	0.979	0.924	10
2023 US Regional Banks	HS	0.0	-0.0333	1.000	1.000	10

*Notes:* Fail is the extreme-period exceedance rate; Gap is  $\mathbb{E}[\text{Loss} - \text{VaR} \mid \text{Loss} > \text{VaR}]$ ; Ratio is  $\mathbb{E}[\min(\text{VaR}/\text{Loss}, 1)]$ ; Score is normalized to  $[0, 1]$ ; K is the number of top losses used.

Table 12 focuses on selected stress episodes over 2018–2023. Performance is regime dependent: QR is strongest in the prolonged drawdown of 2018Q4, whereas FHS dominates in volatility-clustering environments and during abrupt left-tail shocks (February 2018, March 2020), as reflected by both failure rates and gap magnitudes. Event-driven short bursts (election week, 2023 regional banking stress) are adequately handled by HS. These contrasts accord with the mechanism of FHS, which couples nonparametric quantiles with a volatility filter and thus adapts to persistent changes in conditional scale while retaining distributional flexibility.

Overall, the evidence supports two points. First, for nonparametric HS-type models, SNQESA provides a statistically accurate and computationally efficient alternative to bootstrap for constructing VaR intervals: it attains comparable or smaller interval widths at a fraction of the cost, with endpoint error of order  $n^{-1}$ . Second, when combined with a volatility filter (FHS), the approach yields VaR paths with accurate unconditional coverage and stable dynamics across market regimes, including pronounced turbulence, which is desirable for regulatory backtesting and internal risk monitoring.

## 6 Discussion

SNQESA combines a self-normalized pivot with a constrained empirical saddlepoint approximation, thereby avoiding estimation of  $f(q_\tau)$  while aligning tail calibration with the LR/ $r^*$  benchmark. In Monte Carlo experiments spanning light-tailed, heavy-tailed and contaminated mixtures, the continuous equal-tailed inversion maintains coverage close to nominal with competitive lengths and no user tuning. The discrete/exact inversion and the minimum-length variant recover nominal coverage in difficult regimes (extreme  $\tau$  or coarse rounding) at a predictable increase in width, and the interval-score summaries are consistent with these findings.

Our experience supports the continuous equal-tailed procedure as the default, augmented with a mid- $p$  adjustment and a small ridge in the denominator of the self-normalizer. For extreme quantiles or highly discrete outcomes, `SNQESA_disc` or `SNQESA_min`) is preferred; the latter is particularly effective when the score distribution is asymmetric. Reporting both endpoints and interval scores helps reveal when improved coverage is achieved primarily through extra width.

The method requires only sorting and solving a low-dimensional tilted system per endpoint. In rolling windows typical for risk management, the runtime is modest and does not rely on resampling loops or bandwidth searches, which makes uncertainty quantification reproducible and easy to audit.

Coupling SNQESA with historical or filtered historical simulation yields VaR bands with accurate unconditional coverage at moderate computational cost. These bands measure estimation uncertainty of the quantile forecast without committing to a parametric volatility model. Narrower bands produced by parametric specifications do not systematically improve POF/IND/CC backtests in our experiments; by contrast, HS/FHS with SNQESA provides stable traffic-light classifications and clearer diagnostics.

Our theory assumes i.i.d. sampling and local smoothness of  $F$  near  $q_\tau$ . Coverage may deteriorate if the self-normalizer becomes too small (e.g., near a flat empirical step) or when mass accumulates at  $q_\tau$  due to ties/rounding. The ridge safeguards the first case; mid- $p$  and exact inversion address the second. With very small windows and extreme  $\tau$ , information is intrinsically limited for any method; in such

settings we recommend `SNQESA_disc` with conservative tail splitting and to report effective exceedance counts.

Extensions we view as feasible. The rank-reduced curvature of the tilted system and the self-normalization suggest that several directions are attainable with limited changes: (i) two-sample comparisons and pooled designs by replacing the scalar score with the relevant influence function; (ii) regression and panel frameworks (fixed-, random-, and mixed-effects) by plugging in debiased scores and retaining the same constrained tilting step; (iii) weakly dependent data via block/self-normalization of score sums under mixing or martingale-difference assumptions. We expect these extensions to preserve the numerical stability and  $LR/r^*$ -level calibration that make SNQESA effective in finite samples.

## Disclosure Statement

The authors report there are no competing interests to declare.

## Funding

This work was supported by the [Funding Agency] under Grant [number xxxx].

## Appendix A Numerical Details

This appendix records the full constrained ESA computation, including a closed-form Newton step under rank-1 geometry, stable evaluation of cumulants and curvature, line-search and trust-region safeguards, a vanishing ridge near the boundary, continuity corrections, monotone inversion for confidence limits, as well as complexity and error-propagation calculations. All objects are expressed in the unit-scale CGF  $K(\lambda)$  and its derivatives, with the sum-scale recovered by multiplication by  $n$  where needed.

For a fixed threshold  $t \in \mathbb{R}$  write

$$x_{\text{obs}}(t) = \frac{S_n(t)}{\sqrt{Q_n(t)}}, \quad S_n(t) = \sum_{i=1}^n \{\tau - \mathbf{1}(X_i \leq t)\}, \quad Q_n(t) = \sum_{i=1}^n \{\tau - \mathbf{1}(X_i \leq t)\}^2,$$

and impose the boundary in the observed direction

$$g(s, q) = s - x_{\text{obs}}\sqrt{q}.$$

The two-point unit CGF for  $W_i = (\psi_\tau, \psi_\tau^2)^\top$  is

$$M(\lambda) = \tau e^{\lambda_1(\tau-1)+\lambda_2(1-\tau)^2} + (1-\tau)e^{\lambda_1\tau+\lambda_2\tau^2}, \quad K(\lambda) = \log M(\lambda),$$

with tilted success probability

$$p_\lambda = \frac{\tau e^{\lambda_1(\tau-1)+\lambda_2(1-\tau)^2}}{\tau e^{\lambda_1(\tau-1)+\lambda_2(1-\tau)^2} + (1-\tau)e^{\lambda_1\tau+\lambda_2\tau^2}} \in (0, 1),$$

and rank-1 derivatives

$$\mu(\lambda) = \nabla K(\lambda) = (\tau - p_\lambda, \tau^2 + p_\lambda(1 - 2\tau))^\top, \quad \Sigma(\lambda) = \nabla^2 K(\lambda) = p_\lambda(1 - p_\lambda)vv^\top, \quad v = (-1, 1 - 2\tau)^\top.$$

On sum-scale  $J(\lambda) = n\Sigma(\lambda) = np_\lambda(1 - p_\lambda)vv^\top$ . The constrained saddlepoint  $(\hat{\lambda}, \hat{\eta}, \hat{\mu})$  solves

$$F(\lambda, \eta) := \begin{bmatrix} g(n\mu(\lambda)) \\ \lambda - \eta \nabla g(n\mu(\lambda)) \end{bmatrix} = \begin{bmatrix} 0 \\ \mathbf{0} \end{bmatrix}, \quad \nabla g(\mu) = \left( 1, -\frac{x_{\text{obs}}}{2\sqrt{\mu_2}} \right)^\top, \quad H_g(\mu) = \begin{pmatrix} 0 & 0 \\ 0 & \frac{x_{\text{obs}}}{4\mu_2^{3/2}} \end{pmatrix}. \quad (\text{A.1})$$

A damped Newton step  $(\delta\lambda, \delta\eta)$  solves  $DF(\lambda, \eta)[\delta\lambda, \delta\eta] = -F(\lambda, \eta)$  with Jacobian

$$DF(\lambda, \eta) = \begin{bmatrix} \nabla g(n\mu(\lambda))^\top J(\lambda) & 0 \\ I_2 - \eta H_g(n\mu(\lambda))J(\lambda) & -\nabla g(n\mu(\lambda)) \end{bmatrix}.$$

Because  $J(\lambda)$  is rank-1, the Newton system has a closed-form solution by projecting along  $v$ . Let  $\kappa(\lambda) = np_\lambda(1 - p_\lambda)$  so that  $J(\lambda) = \kappa v v^\top$ , and define

$$\gamma(\lambda) = \nabla g(n\mu(\lambda)) \cdot v, \quad \zeta(\lambda) = v^\top H_g(n\mu(\lambda))v = \frac{x_{\text{obs}}}{4} \cdot \frac{(1 - 2\tau)^2}{(n\mu_2(\lambda))^{3/2}}.$$

With residuals  $r_0 = g(n\mu(\lambda))$  and  $r_1 = \lambda - \eta \nabla g(n\mu(\lambda))$ , the first Newton equation gives

$$v^\top \delta\lambda = -\frac{r_0}{\kappa\gamma}, \quad \alpha := \frac{v^\top \delta\lambda}{\|v\|^2} = -\frac{r_0}{\kappa\gamma\|v\|^2}, \quad \delta\lambda = \alpha v + z, \quad z \perp v. \quad (\text{A.2})$$

The second equation reduces to

$$\alpha v + z - \eta\kappa\alpha\|v\|^2 H_g v - \nabla g \delta\eta = -r_1. \quad (\text{A.3})$$

Left-multiplying (A.3) by  $\nabla g^\top$  yields

$$-\|\nabla g\|^2 \delta\eta + \alpha\gamma + \nabla g \cdot z - \eta\kappa\alpha\|v\|^2 \nabla g \cdot (H_g v) = -\nabla g \cdot r_1. \quad (\text{A.4})$$

Setting  $z \equiv 0$  gives the explicit update

$$\delta\eta = \frac{\nabla g \cdot r_1 - \alpha\gamma + \eta\kappa\alpha\|v\|^2 \nabla g \cdot (H_g v)}{\|\nabla g\|^2}, \quad \delta\lambda = \alpha v. \quad (\text{A.5})$$

If one prefers to remove residual components orthogonal to  $\text{span}\{v, \nabla g\}$ , a correction  $z$  may be computed from (A.3) as

$$z = -r_1 - \alpha v + \eta\kappa\alpha\|v\|^2 H_g v + \nabla g \delta\eta, \quad z \leftarrow z - \frac{v^\top z}{\|v\|^2} v, \quad (\text{A.6})$$

which enforces  $z \perp v$  and preserves stability even when  $H_g$  is large ( $\mu_2 \downarrow 0$ ).

The raw Newton increment is damped by a backtracking line-search with factor  $\rho \in (0, 1)$  (we use  $\rho = 1/2$ ), decreasing the merit

$$\Psi(\lambda, \eta) = \frac{1}{2} r_0^2 + \frac{1}{2} \|r_1\|^2, \quad (\text{A.7})$$

until  $\Psi$  decreases (Armijo condition suffices). A maximal damping factor of 10 avoids excessive shortening. To keep the tilt interior we enforce

$$p_\lambda \in [\varepsilon, 1 - \varepsilon], \quad \varepsilon = 10^{-10},$$

either by a logistic reparameterization  $\beta = \text{logit}(p_\lambda)$  or by rejecting steps that violate the interval; both are equivalent since  $\nabla p_\lambda = p_\lambda(1 - p_\lambda)v$  is collinear with  $v$ . We also bound  $|\hat{\eta}|$  via a trust-region on  $(\lambda, \eta)$  to prevent overflow when  $\nabla g(\hat{\mu}) \cdot v$  is near zero.

Near extreme quantiles or very small  $n$  we stabilize  $x_{\text{obs}}$  and  $\nabla g$  by a vanishing ridge

$$Q_n(t) \leftarrow Q_n(t) + \epsilon_n, \quad \epsilon_n \rightarrow 0, \quad (\text{A.8})$$

and in practice set  $\epsilon_n = cn^{-1/2}$  with a small constant  $c$ . A first-order Taylor expansion gives

$$x_{\text{obs}}^{(\text{ridge})} - x_{\text{obs}} = \frac{S_n}{\sqrt{Q_n + \epsilon_n}} - \frac{S_n}{\sqrt{Q_n}} = -\frac{S_n \epsilon_n}{2Q_n^{3/2}} + O\left(\frac{\epsilon_n^2}{Q_n^{5/2}}\right),$$

and under  $H_0$ ,  $S_n = O_p(n^{1/2})$  and  $Q_n = n\tau(1 - \tau) + O_p(n^{1/2})$ , whence

$$x_{\text{obs}}^{(\text{ridge})} - x_{\text{obs}} = O_p(n^{-3/2}), \quad (\text{A.9})$$

which is negligible relative to the  $n^{-1/2}$  scale of tail arguments and does not affect second-order coverage.

Tail areas are computed from the sum-scale signed root deviance

$$D_{\text{sum}} = 2n\{\hat{\lambda}^\top \mu(\hat{\lambda}) - K(\hat{\lambda})\}, \quad r = \text{sgn}(\hat{\eta})\sqrt{D_{\text{sum}}},$$

and curvature terms. Skovgaard's rank-1 form

$$w = |\hat{\eta}| \frac{\sqrt{\text{pdet}(J(\hat{\lambda}))} \|\nabla g(\hat{\mu})\|}{(\nabla g(\hat{\mu})^\top \Sigma(\hat{\lambda})^+ \nabla g(\hat{\mu}))^{1/2}}$$

reduces here to the closed expression

$$w = |\hat{\eta}| \sqrt{np_{\hat{\lambda}}(1-p_{\hat{\lambda}})} \frac{\|v\|^3 \|\nabla g(\hat{\mu})\|}{|\nabla g(\hat{\mu}) \cdot v|}, \quad (\text{A.10})$$

since  $\text{pdet}(J) = np_{\hat{\lambda}}(1-p_{\hat{\lambda}})\|v\|^2$  and  $\Sigma(\hat{\lambda})^+ = \{p_{\hat{\lambda}}(1-p_{\hat{\lambda}})\}^{-1}vv^\top/\|v\|^4$  imply  $\nabla g(\hat{\mu})^\top \Sigma(\hat{\lambda})^+ \nabla g(\hat{\mu}) = \{(\nabla g(\hat{\mu}) \cdot v)^2\}/\{p_{\hat{\lambda}}(1-p_{\hat{\lambda}})\|v\|^4\}$ . We also use the signed Lugannani-Rice quantity

$$q^\pm = (\text{logit}(\hat{p}) - \text{logit}(\tau)) \sqrt{n\hat{p}(1-\hat{p})}. \quad (\text{A.11})$$

The Barndorff-Nielsen correction

$$r^* = r + \frac{1}{r} \log \frac{r}{w}$$

is used if  $|\log(r/w)| \leq c_0$  (default  $c_0 = 2$ ); otherwise the signed Lugannani-Rice approximation

$$p_{\text{dir}}(t) \approx \Phi(-\text{sgn}(x_{\text{obs}})r) + \phi(r) \left( \frac{1}{r} - \frac{1}{q^\pm} \right)$$

is applied to the observed tail. Because under  $H_0$  the statistic is a monotone transform of a binomial mean, we evaluate tails by default with a mid-p modification

$$p_{\text{mid}}(t) = \mathbb{P}\{T_n(t) > x_{\text{obs}}(t)\} + \frac{1}{2} \mathbb{P}\{T_n(t) = x_{\text{obs}}(t)\},$$

or with a small Cornish-Fisher continuity shift; both preserve the  $O(n^{-1})$  coverage error when combined with third-order tail accuracy.

For stable floating-point evaluation write  $K(\lambda) = \log\{\tau e^A + (1-\tau)e^B\}$  with  $A = \lambda_1(\tau-1) + \lambda_2(1-\tau)^2$ ,  $B = \lambda_1\tau + \lambda_2\tau^2$ , and use log-sum-exp

$$m = \max\{A, B\}, \quad K(\lambda) = m + \log(\tau e^{A-m} + (1-\tau)e^{B-m}),$$

and compute  $\hat{\lambda}^\top \mu(\hat{\lambda}) - K(\hat{\lambda})$  with `log1p` and `expm1` to reduce cancellation. The Kullback-Leibler divergence and logit difference are evaluated as

$$\text{KL}(u\|\tau) = u \log\left(1 + \frac{u-\tau}{\tau}\right) + (1-u) \log\left(1 - \frac{u-\tau}{1-\tau}\right), \quad \text{logit}(u) - \text{logit}(\tau) = \log \frac{u(1-\tau)}{\tau(1-u)}.$$

For large positive  $z$ , compute  $\Phi(-z)$  as  $\frac{1}{2}\text{erfc}(z/\sqrt{2})$ ; if a log-tail is needed,

$$\log \Phi(-z) = -\frac{z^2}{2} - \log z - \frac{1}{2} \log(2\pi) + \log\left(1 - \frac{1}{z^2} + \frac{3}{z^4} - \dots\right).$$

The one-dimensional fallback relies on the strictly monotone transform

$$h(u) = \frac{\sqrt{n}(\tau-u)}{\sqrt{u(1-\tau)^2 + (1-u)\tau^2}}, \quad d(u) = \tau^2 + u(1-2\tau),$$

whose derivatives are

$$h'(u) = -\frac{\sqrt{n}}{2d(u)^{3/2}} \{(1-2\tau)u + \tau\} < 0, \quad h''(u) = \frac{3\sqrt{n}(1-2\tau)\{(1-2\tau)u + \tau\}}{4d(u)^{5/2}}.$$

Given  $x_{\text{obs}}$ , solve  $h(u) = x_{\text{obs}}$  for  $u_x \in (0, 1)$  by safeguarded Newton

$$u^{(k+1)} = \Pi_{(a,b)} \left\{ u^{(k)} - \frac{h(u^{(k)}) - x_{\text{obs}}}{h'(u^{(k)})} \right\}, \quad (a, b) = (10^{-12}, 1 - 10^{-12}),$$

with bisection if the Newton step fails the interval-shrinking test, and then evaluate the binomial signed LR quantities at  $u_x$ :

$$r = \text{sgn}(u_x - \tau) \sqrt{2n\text{KL}(u_x\|\tau)}, \quad q^\pm = (\text{logit}(u_x) - \text{logit}(\tau)) \sqrt{n u_x (1-u_x)}.$$

Confidence limits are obtained by inverting the directed tails. Writing  $f_{\downarrow}(t) = p_{\downarrow}(t) - \alpha/2$  and  $f_{\uparrow}(t) = p_{\uparrow}(t) - \alpha/2$ , monotonicity of  $p_{\downarrow}$  on  $(-\infty, \hat{q}_\tau]$  and of  $p_{\uparrow}$  on  $[\hat{q}_\tau, \infty)$  permits bracketing  $t_L$  and  $t_U$  by

scanning ordered  $\{X_{(k)}\}$  until a sign change, and refining by bisection to  $|t_{k+1} - t_k| < 10^{-8}$ . With ties or discretization we use the mid-p or a Cornish-Fisher shift; both preserve the  $O(n^{-1})$  coverage when combined with third-order tails.

We summarize complexity. Sorting the sample once costs  $O(n \log n)$ . Along the sorted path,  $S_n$  and  $Q_n$  admit  $O(1)$  updates between adjacent order statistics because  $S_n$  changes by  $\pm(1 - \tau)$  and  $Q_n$  by a deterministic affine increment; scanning to bracket each endpoint is  $O(n)$  in the worst case and much less in practice. Each  $p$ -value evaluation solves a  $3 \times 3$  nonlinear system with rank-1 linear algebra; the number of Newton steps is bounded by a small constant due to damping, hence  $O(1)$  per evaluation. Bisection requires  $O(\log(1/\text{tol}))$  steps (with  $\text{tol} = 10^{-8}$  this is at most 27). Therefore, the overall complexity for a single  $(1 - \alpha)$  CI is  $O(n \log n)$  dominated by sorting.

Finally we quantify error propagation. Let  $p^*(t)$  denote the exact directed tail and  $\tilde{p}(t)$  the ESA approximation. For the one-parameter binomial tilt, the signed Lugannani-Rice tail error satisfies

$$\sup_{|r| \leq C} |p^* - \tilde{p}_{\text{LR}}| = O(n^{-3/2}), \quad \sup_{|r| \leq C} \frac{|p^* - \tilde{p}_{r^*}|}{p^*} = O(n^{-3/2}),$$

uniformly on compact  $r$ -sets, and by algebraic equivalence the same orders hold for the constrained rank-1 construction. Passing from  $p$  to an endpoint  $t$  near  $q_\tau$  introduces the local scale  $f(q_\tau)^{-1}$ . With  $F(t) = \tau + f(q_\tau)(t - q_\tau) + O((t - q_\tau)^2)$  and

$$z(t) = \frac{\sqrt{n}(F(t) - \tau)}{\sqrt{\tau(1 - \tau)}}, \quad p^*(t) = \Phi(-z(t)) + O(n^{-1}),$$

one has at  $t = q_\tau$  the sensitivity

$$\frac{dp^*}{dt} \Big|_{t=q_\tau} = -\phi(0) \frac{\sqrt{n}f(q_\tau)}{\sqrt{\tau(1 - \tau)}}.$$

Therefore a tail error  $\Delta p(t) = \tilde{p}(t) - p^*(t) = O(n^{-3/2})$  transfers to an endpoint perturbation

$$\Delta t = -\frac{\Delta p}{p^{*\prime}(q_\tau)} + o(\Delta p) = O\left(\frac{1}{n}\right) \cdot \frac{\sqrt{2\pi\tau(1 - \tau)}}{f(q_\tau)},$$

so the coverage error of the inverted CI is  $O(n^{-1})$ . The ridge perturbation (A.9) induces a tail change of order  $O_p(n^{-3/2})$  and therefore an endpoint impact of order  $O_p(n^{-2})$ , asymptotically negligible. In extreme-quantile regimes with  $\tau = \tau_n$  satisfying  $\min\{n\tau_n, n(1 - \tau_n)\} \rightarrow \infty$ , all rates remain valid uniformly over compact  $r$ -sets; choosing  $\epsilon_n = cn^{-1/2}$  keeps the orders unchanged.

Collecting identities used by curvature terms, the pseudo-determinant and generalized inverse are

$$\text{pdet}(\Sigma(\lambda)) = p_\lambda(1 - p_\lambda)\|v\|^2, \quad \Sigma(\lambda)^+ = \frac{vv^\top}{p_\lambda(1 - p_\lambda)\|v\|^4},$$

so any expression originally involving  $\det \Sigma$  or  $\Sigma^{-1}$  is read along  $\text{span}(v)$  by replacing them with  $\text{pdet}$  and  $\Sigma^+$ . With these definitions, the entire tail evaluation at a fixed  $t$  follows

- compute  $x_{\text{obs}}$ , solve (A.1) via (A.2)-(A.6) with damping and trust-region
- evaluate  $(r, w, q^\pm)$  then signed  $r^*$  or LR tail

with a one-dimensional fallback through  $h^{-1}$  and a degeneracy check  $|\nabla g(\hat{\mu}) \cdot v| > \delta$  (we use  $\delta = 10^{-10}$ ); if violated we switch to the binomial evaluation at  $u_x$  for both  $r^*$  and LR tails.

## Appendix B Proofs for Section 3

We collect detailed proofs for Lemma 1 and Theorems 1-4. Throughout, recall the definitions in Sections 2 and 3. All limits are taken as  $n \rightarrow \infty$  unless stated otherwise.

*Proof of Lemma 1.* By definition,

$$S_n(t) = \sum_{i=1}^n \{\tau - Y_i(t)\} = n\{\tau - \bar{Y}_n(t)\},$$

and

$$Q_n(t) = \sum_{i=1}^n \{\tau - Y_i(t)\}^2 = \sum_{i=1}^n [Y_i(t)(1-\tau)^2 + \{1-Y_i(t)\}\tau^2] = n\{\bar{Y}_n(t)(1-\tau)^2 + \{1-\bar{Y}_n(t)\}\tau^2\}.$$

Therefore

$$T_n(t) = \frac{S_n(t)}{\sqrt{Q_n(t)}} = \frac{\sqrt{n}\{\tau - \bar{Y}_n(t)\}}{\sqrt{\bar{Y}_n(t)(1-\tau)^2 + \{1-\bar{Y}_n(t)\}\tau^2}} = h(\bar{Y}_n(t)), \quad (\text{B.1})$$

with  $h$  given in (12). Differentiation yields  $h'(u) = -\sqrt{n}\{(1-2\tau)u + \tau\}/\{2d(u)^{3/2}\} < 0$  on  $(0, 1)$ , so  $h$  is strictly decreasing and continuous. For any  $x \in \mathbb{R}$  the equation  $h(u) = x$  has a unique solution  $u_x = h^{-1}(x) \in (0, 1)$ , and since  $h$  is decreasing,

$$\{T_n(t) \geq x\} = \{h(\bar{Y}_n(t)) \geq x\} = \{\bar{Y}_n(t) \leq u_x\}.$$

This proves the lemma.  $\square$

*Proof of Theorem 1.* Fix  $t$  and denote  $\bar{Y}_n = \bar{Y}_n(t)$ . Under  $H_0 : F(t) = \tau$  we have  $\bar{Y}_n = n^{-1}\text{Bin}(n, \tau)$ . By Lemma 1,

$$\mathbb{P}\{T_n(t) \geq x\} = \mathbb{P}\{\bar{Y}_n \leq u_x\}, \quad u_x = h^{-1}(x). \quad (\text{B.2})$$

Write  $S = \sum_{i=1}^n Y_i$ , so  $S \sim \text{Bin}(n, \tau)$  and  $\bar{Y}_n = S/n$ . The CGF of  $S$  is

$$K_S(\theta) = \log \mathbb{E}[e^{\theta S}] = n \log \{(1-\tau) + \tau e^\theta\}. \quad (\text{B.3})$$

Let  $s = nu_x$ . The saddlepoint  $\hat{\theta}$  solves  $K'_S(\hat{\theta}) = s$ , i.e.

$$\frac{d}{d\theta} K_S(\theta) \Big|_{\theta=\hat{\theta}} = n \cdot \frac{\tau e^{\hat{\theta}}}{(1-\tau) + \tau e^{\hat{\theta}}} = s, \quad (\text{B.4})$$

so the tilted success probability equals  $u_x$ :

$$\hat{p} := \frac{\tau e^{\hat{\theta}}}{(1-\tau) + \tau e^{\hat{\theta}}} = u_x. \quad (\text{B.5})$$

The signed one-parameter saddlepoint scalars for the lower tail  $\mathbb{P}\{S \leq s\}$  are

$$r = \text{sgn}(u_x - \tau) \sqrt{2n \text{KL}(u_x \parallel \tau)}, \quad q^\pm = (\text{logit}(u_x) - \text{logit}(\tau)) \sqrt{n u_x (1 - u_x)}, \quad (\text{B.6})$$

and the Lugannani-Rice and Barndorff-Nielsen forms give, uniformly on compact  $r$ -sets,

$$\mathbb{P}\{S \leq s\} = \Phi(r) + \phi(r) \left( \frac{1}{r} - \frac{1}{q^\pm} \right) + O(n^{-3/2}), \quad \mathbb{P}\{S \leq s\} = \Phi(r^*) \{1 + O(n^{-3/2})\}. \quad (\text{B.7})$$

By (B.2)-(B.7), for  $x = x_{\text{obs}}(t)$  with sign directing the observed tail,

$$p_{\text{dir}}(t) = \begin{cases} \Phi(r) + \phi(r) \left( \frac{1}{r} - \frac{1}{q^\pm} \right) + O(n^{-3/2}), & x \geq 0, \\ \Phi(-r) + \phi(r) \left( \frac{1}{r} - \frac{1}{q^\pm} \right) + O(n^{-3/2}), & x < 0, \end{cases} \quad (\text{B.8})$$

which can be summarized as  $p_{\text{dir}}(t) = \Phi(-\text{sgn}(x)r) + \phi(r)(1/r - 1/q^\pm) + O(n^{-3/2})$ . For the constrained rank-1 ESA we have  $\hat{\mu} = (\tau - \hat{p}, \tau^2 + \hat{p}(1-2\tau))^\top$  and the boundary  $g(\hat{\mu}) = 0$  reads

$$\tau - \hat{p} = x_{\text{obs}} \sqrt{\tau^2 + \hat{p}(1-2\tau)}. \quad (\text{B.9})$$

Hence  $h(\hat{p}) = x_{\text{obs}}$  and, by strict monotonicity of  $h$ ,  $\hat{p} = u_x$ . Therefore the constrained deviance,  $r$ ,  $q^\pm$  and  $r^*$  match the binomial ones, which proves (15)-(16).  $\square$

*Proof of Theorem 2.* Let  $p^*(t)$  denote the exact directed tail at  $t$ , and  $\tilde{p}(t)$  the ESA approximation from Theorem 1. Near  $t = q_\tau$ ,

$$p^*(t) = \Phi(-z(t)) + O(n^{-1}), \quad z(t) = \frac{\sqrt{n}\{F(t) - \tau\}}{\sqrt{\tau(1 - \tau)}}, \quad (\text{B.10})$$

uniformly for  $t$  in a shrinking neighborhood of  $q_\tau$ . Differentiating at  $t = q_\tau$  gives

$$\frac{dp^*}{dt} \Big|_{t=q_\tau} = -\phi(0) \frac{\sqrt{n}f(q_\tau)}{\sqrt{\tau(1 - \tau)}}. \quad (\text{B.11})$$

By Theorem 1,  $\tilde{p}(t) = p^*(t) + \Delta_n(t)$  with

$$\sup_{|r| \leq C} |\Delta_n(t)| = O(n^{-3/2}), \quad (\text{B.12})$$

uniformly in  $t$  such that the directed  $r$  lies in a compact set. Consider the lower endpoint  $t_L$  defined by  $p_\downarrow(t_L) = \alpha/2$ ; write  $t_L^*$  for the exact solution and  $\tilde{t}_L$  for the ESA solution. A first-order expansion of  $p^*$  around  $t_L^*$  together with (B.11) and (B.12) yields

$$\tilde{t}_L - t_L^* = \frac{\Delta_n(\tilde{t}_L)}{p'^*(t_L^*)} + o(\Delta_n) = O\left(\frac{1}{n}\right) \cdot \frac{\sqrt{\tau(1 - \tau)}}{f(q_\tau)\phi(0)} = O(n^{-1}), \quad (\text{B.13})$$

and similarly for the upper endpoint  $t_U$ . Therefore the ESA interval differs from the exact equal-tailed interval by  $O(n^{-1})$  at each endpoint, and the coverage error satisfies the same order; the uniformity over classes with  $f(q_\tau)$  bounded and bounded away from zero follows from the uniformity in (B.12) and the monotonicity of the directed tails.  $\square$

*Proof of Theorem 3.* Under  $H_0$ , the bivariate variable  $W_i = (\psi_\tau, \psi_\tau^2)$  has a two-point distribution supported on  $w_0 = (\tau, \tau^2)^\top$  and  $w_1 = (\tau - 1, (1 - \tau)^2)^\top$ . Hence its MGF and CGF exist for all arguments regardless of the tail behavior of  $X$ , and the rank-1 derivatives are always well defined. The third-order tail accuracy (15)-(16) and the coverage order (19) only require the binomial reduction of Lemma 1 and the local continuity  $f(q_\tau) > 0$  to linearize  $F(t)$  near  $q_\tau$ . No global moment assumptions on  $X$  are used. Therefore the stated robustness holds.  $\square$

*Proof of Theorem 4.* Let  $\tau = \tau_n$  with  $\min\{n\tau_n, n(1 - \tau_n)\} \rightarrow \infty$ . Then the effective information  $n\tau_n(1 - \tau_n)$  diverges, and the one-parameter binomial saddlepoint expansions (B.7) hold uniformly on compact  $r$ -sets. By Lemma 1 and the identity  $\hat{p} = u_x$ , the constrained rank-1 ESA inherits the same scalars  $r$ ,  $q^\pm$  and  $r^*$  uniformly, establishing (15)-(16) for  $\tau_n$ .

For coverage, write  $z(t)$  as in (B.10) with  $\tau$  replaced by  $\tau_n$ , so that  $z'(q_{\tau_n})$  is of order  $\sqrt{n\tau_n(1 - \tau_n)}f(q_{\tau_n})$ . The same linearization argument as in (B.13) shows that endpoint errors remain  $O(n^{-1})$  uniformly as long as  $f(q_{\tau_n})$  stays bounded and bounded away from zero on a neighborhood of  $q_{\tau_n}$ . If a vanishing ridge  $Q_n \leftarrow Q_n + \epsilon_n$  is used with  $\epsilon_n \rightarrow 0$  (e.g.  $\epsilon_n = cn^{-1/2}$ ), the perturbation of  $x_{\text{obs}}$  is  $O_p(n^{-3/2})$  as in (A.9) and therefore negligible for both third-order tails and second-order endpoints. This proves the theorem.  $\square$

## References

Abd El-Raheem, A. E.-R. M., Hosny, M., and Abd-Elfattah, E. F. (2023). Statistical inference of the class of nonparametric tests for the panel count and current status data from the perspective of the saddlepoint approximation. *Journal of Mathematics*, 2023.

Barndorff-Nielsen, O. E. (1986). Inference on full or partial parameters based on the standardized signed log likelihood ratio. *Biometrika*, 73(2):307–322.

Bickel, P. J. and Sakov, A. (2008). On the choice of  $m$  in the  $m$  out of  $n$  bootstrap and confidence bounds for extrema. *Statistica Sinica*, 18(3):967–985.

Brazzale, A. R., Davison, A. C., and Reid, N. (2007). *Applied Asymptotics: Case Studies in Small-Sample Statistics*. Cambridge University Press, Cambridge.

Butler, R. W. (2007). *Saddlepoint Approximations with Applications*. Cambridge University Press, Cambridge.

Chen, S. X. and Hall, P. (1993). Smoothed empirical likelihood confidence intervals for quantiles. *The Annals of Statistics*, 21(3):1166–1181.

Cheng, C. H. and Chan, K. W. (2024). A general framework for constructing locally self-normalized multiple-change-point tests. *Journal of Business & Economic Statistics*, 42(2):719–731.

Chernozhukov, V., Fernández-Val, I., and Kaji, T. (2017). Extremal quantile regression: An overview. In Koenker, R., Chernozhukov, V., He, X., and Peng, L., editors, *Handbook of Quantile Regression*, pages 257–288. Chapman & Hall/CRC, Boca Raton.

Chernozhukov, V., Fernández-Val, I., and Kato, K. (2011). Inference for extremal conditional quantile models, with an application to market and birthweight risks. *The Review of Economic Studies*, 78(2):559–589.

Christoffersen, P. F. (1998). Evaluating interval forecasts. *International Economic Review*, 39(4):841–862.

Daniels, H. E. (1954). Saddlepoint approximations in statistics. *The Annals of Mathematical Statistics*, 25(4):631–650.

Davison, A. C. and Hinkley, D. V. (1997). *Bootstrap Methods and their Application*. Cambridge University Press, Cambridge.

de la Peña, V. H., Lai, T. L., and Shao, Q.-M. (2009). *Self-Normalized Processes: Limit Theory and Statistical Applications*. Springer, Berlin.

Doukhan, P. (1994). *Mixing: Properties and Examples*, volume 85 of *Lecture Notes in Statistics*. Springer, New York.

Efron, B. (1987). Better bootstrap confidence intervals. *Journal of the American Statistical Association*, 82(397):171–185.

Efron, B. and Tibshirani, R. J. (1993). *An Introduction to the Bootstrap*. Chapman & Hall/CRC, New York.

Feuerverger, A. (1989). On the empirical saddlepoint approximation. *Biometrika*, 76(3):457–464.

Hall, P. and Sheather, S. J. (1988). On the distribution of a studentized quantile. *Journal of the Royal Statistical Society: Series B (Methodological)*, 50(3):381–391.

Holcblat, B. and Vitale, C. (2022). The empirical saddlepoint estimator. *Electronic Journal of Statistics*, 16(1):2499–2540.

Hyndman, R. J. and Fan, Y. (1996). Sample quantiles in statistical packages. *The American Statistician*, 50(4):361–365.

Jensen, J. L. (1995). *Saddlepoint Approximations*. Oxford Statistical Science Series. Oxford University Press, Oxford.

Jiang, C., La Vecchia, D., Ronchetti, E., and Scaillet, O. (2023). Saddlepoint approximations for spatial panel data models. *Journal of the American Statistical Association*, 118(542):1164–1175.

Jing, B.-Y., Shao, Q.-M., and Wang, Q. (2003). Self-normalized cramér-type moderate deviations for independent random variables. *The Annals of Probability*, 31(4):2167–2215.

Ko, S., German, C. A., Jensen, A., Shen, J., Wang, A., Mehrotra, D. V., Sun, Y. V., Sinsheimer, J. S., Zhou, H., and Zhou, J. J. (2022). Gwas of longitudinal trajectories at biobank scale. *The American Journal of Human Genetics*, 109(3):433–445.

Koenker, R. (2005). *Quantile Regression*. Econometric Society Monographs. Cambridge University Press, Cambridge.

Koenker, R. and Bassett, G. (1978). Regression quantiles. *Econometrica*, 46(1):33–50.

Kolassa, J. E. (2006). *Series Approximation Methods in Statistics*. Springer, New York.

Kupiec, P. H. (1995). Techniques for verifying the accuracy of risk measurement models. *The Journal of Derivatives*, 3(2):73–84.

Liu, X., Long, W., Peng, L., and Yang, B. (2024). A unified inference for predictive quantile regression. *Journal of the American Statistical Association*, 119(546):1526–1540.

Lugannani, R. and Rice, S. (1980). Saddle point approximation for the distribution of the sum of independent random variables. *Advances in Applied Probability*, 12(2):475–490.

Owen, A. B. (2001). *Empirical Likelihood*. Chapman & Hall/CRC, Boca Raton.

Politis, D. N., Romano, J. P., and Wolf, M. (1999). *Subsampling*. Springer, New York.

Reid, N. (2003). Asymptotics and the theory of inference. *Annals of Statistics*, 31(6):1695–1731.

Rio, E. (2000). *Théorie asymptotique des processus aléatoires faiblement dépendants*, volume 31 of *Mathématiques & Applications*. Springer, Berlin. In French.

Serfling, R. J. (1980). *Approximation Theorems of Mathematical Statistics*. John Wiley & Sons, New York.

Shao, X. (2010). A self-normalized approach to confidence interval construction in time series. *Journal of the Royal Statistical Society: Series B (Statistical Methodology)*, 72(3):343–366.

Shao, X. (2015). Self-normalization for time series: A review of recent developments. *Journal of the American Statistical Association*, 110(512):1797–1817.

Sheather, S. J. (2004). Density estimation. *Statistical Science*, 19(4):588–597.

Sheather, S. J. and Jones, M. C. (1991). A reliable data-based bandwidth selection method for kernel density estimation. *Journal of the Royal Statistical Society: Series B (Methodological)*, 53(3):683–690.

Skovgaard, I. M. (2001). Likelihood asymptotics. *Scandinavian Journal of Statistics*, 28(1):3–32.

van der Vaart, A. W. and Wellner, J. A. (1996). *Weak Convergence and Empirical Processes: With Applications to Statistics*. Springer Series in Statistics. Springer, New York.